# The role of microRNA alterations in post-ischemic neovascularization

Kwast, R.V.C.T. van der

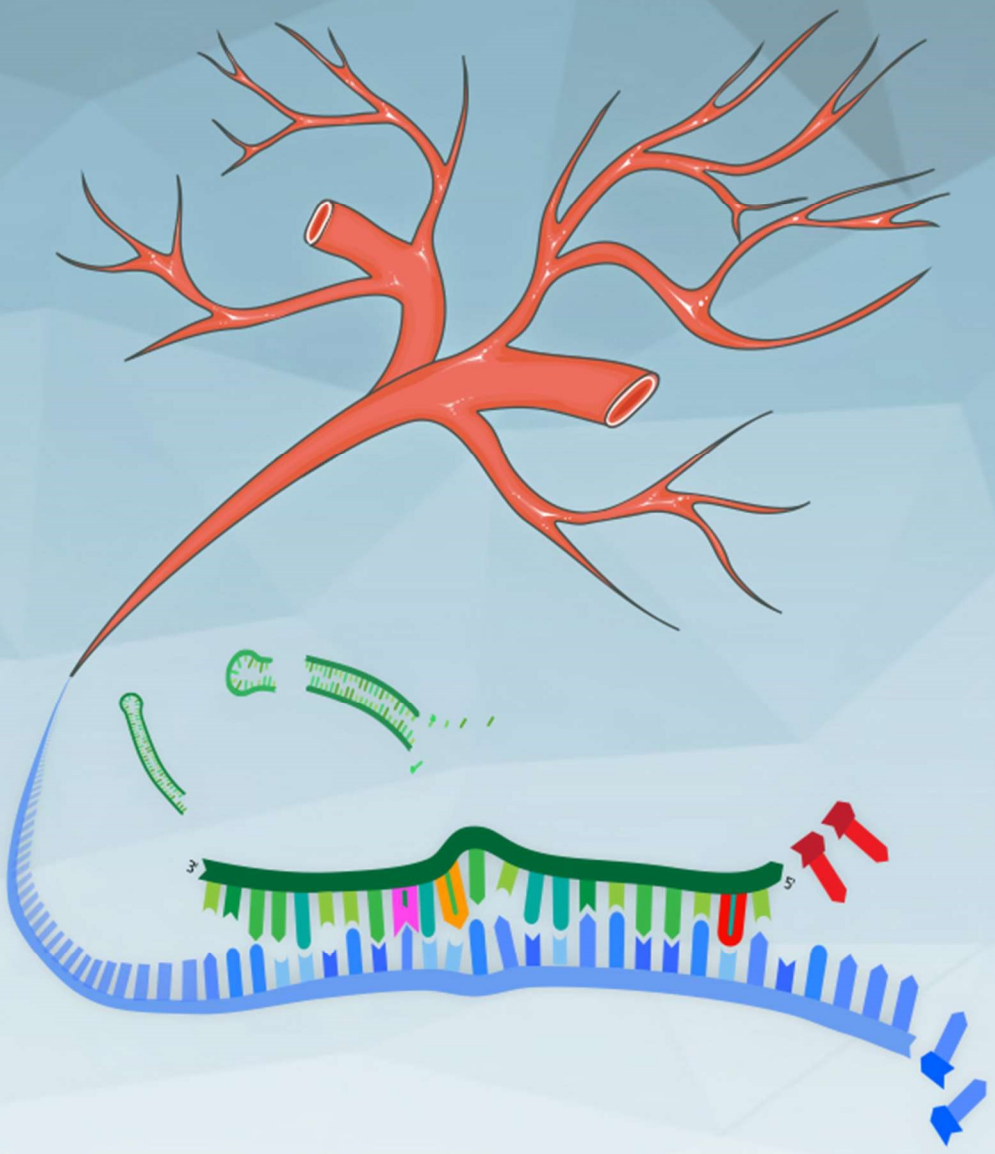
3'
5'

# CHAPTER 4

## A-to-I editing of microRNA-487b alters target gene selection after ischemia and promotes neovascularization

Reginald V.C.T. van der Kwast
Eva van Ingen
Laura Parma
Hendrika A.B. Peters
Paul H.A. Quax
A. Yaël Nossent

*Circulation Research 2018 Feb 2;122(3):444-456*

## ABSTRACT

*Rationale.* Adenosine-to-inosine (A-to-I) editing of microRNAs has the potential to cause a shift in target-site selection. 2'-O-ribose-methylation (2'OMe) of adenosine residues however, has been shown to inhibit A-to-I editing.

*Objective.* To investigate whether angiomiR miR487b is subject to A-to-I editing and/or 2'OMe during neovascularization.

*Methods and Results.* cDNA was prepared from C57BL/6-mice subjected to hindlimb ischemia. Using Sanger-sequencing and endonuclease digestion, we identified and validated A-to-I editing of the miR487b seed-sequence. In the gastrocnemius muscle, pri-miR487b editing increased from 6.7±0.4% before to 11.7±1.6% (*P*=0.02) 1 day after ischemia. Edited pri-miR487b is processed into a novel microRNA, miR487b-ED, which is also upregulated following ischemia. We confirmed editing of miR487b in multiple human primary vascular cell-types. siRNA-mediated knockdown demonstrated that editing is ADAR1&2-dependent.

Using 'Reverse-Transcription at Low dNTP concentrations followed by Quantitative-PCR' (RTL-Q), we found that the same adenosine-residue is methylated in mice and human primary cells. In the murine gastrocnemius, the estimated methylation fraction increased from 32.8±14% before to 53.6±12% 1 day after ischemia. siRNA knockdown confirmed that methylation is Fibrillarin-dependent. Although we could not confirm that methylation directly inhibits editing, we do show that ADAR1&2 and Fibrillarin negatively influence each other's expression.

Using multiple luciferase reporter gene assays, we could demonstrate that editing results in a complete switch of target-site selection. In human primary cells, we confirmed the shift in miR487b targeting after editing, resulting in a miR487b-ED targetome that is enriched for multiple pro-angiogenic pathways. Furthermore, overexpression of miR-487b-ED, but not miR-487b-WT, stimulates angiogenesis in both *in vitro* and *ex vivo* assays.

*Conclusions.* MiR487b is edited in the seed-sequence in mice and humans, resulting in a novel, pro-angiogenic microRNA with a unique targetome. The rate of miR487b editing, as well as 2'OMe, is increased in murine muscle tissue during post-ischemic neovascularization. Our findings suggest miR487b editing plays an intricate role in post-ischemic neovascularization.

## NOVELTY AND SIGNIFICANCE

***What Is Known?***

- The multifactorial process of neovascularization is crucial for blood flow recovery after cardiovascular events and can be regulated by endogenous microRNAs, which each regulate the expression of multiple neovascularization-related genes.
- MicroRNA-487b (miR487b) has very few putative target genes compared to other vasoactive microRNAs, but is still able to regulate bloodflow recovery after hindlimb ischemia, as well as arterial wall integrity during chronic hypertension *in vivo*.
- MicroRNAs can be subject to adenosine-to-inosine (A-to-I) editing by adenosine deaminase acting on RNA enzymes (ADARs). Should A-to-I editing occur in the seed sequence of the microRNA, this could alter the microRNA's target site recognition and hence its target gene selection.

***What New Information Does This Article Contribute?***

- We provide the first evidence of active regulation of microRNA A-to-I-editing during ischemia by demonstrating that a fraction of miR487b is edited by ADARs in its seed sequence, and that the rate of editing is increased during blood flow recovery after ischemia *in vivo*.
- The same adenosine residue that is subject to editing, can also be 2'-O-ribose-methylated by Fibrillarin. The methylation rate also increased during ischemia *in vivo* even though ADARs and Fibrillarin were found to negatively influence each other's expression *in vitro*.
- The edited miR487b (miR487b-ED) binds to and represses a completely different set of genes than the unedited miR487b (miR487b-WT). Because of this switch in 'targetome', miR487b-ED now promotes angiogenesis and neovascularization, whereas miR487b-WT does not.

The 14q32 microRNA gene cluster has been shown to regulate the complex, multifactorial process of neovascularization by modulating expression of multiple, rather than a single, target genes. MiR487b is also able to regulate blood flow recovery after ischemia, even though, compared to other vasoactive 14q32 microRNAs, miR487b has a strikingly small putative targetome. We hypothesized that the miR487b targetome is expanded or altered during neovascularization through A-to-I-editing of the seed-sequence. We demonstrated that a fraction of the miR487b transcript, pri-miR487b, is indeed subject to A-to-I-editing by ADAR enzymes in both mice and humans. The edited pri-miR487b is processed into a mature pro-angiogenic microRNA with a novel, unique seed sequence, miR487b-ED.The rate of editing is increased during blood flow recovery after ischemia *in vivo* in mice. Previous studies showed that 2'-O-ribose-methylation of adenosines can inhibit A-to-I-editing, but while the miR487b-adenosine that is subject to editing was shown to be 2'-O-ribose-methylated, the methylation-rate followed the same the pattern as the editing-rate *in vivo*. Our findings show that A-to-I-editing can actively change microRNA-functionality during vascular remodeling. As many other microRNAs may be subject to editing as well, editing can have major implications for future microRNA-research and even for future microRNA-based therapeutics.

## INTRODUCTION

Neovascularization is the body's natural repair mechanism to restore blood flow to ischemic tissues. Neovascularization is comprised of angiogenesis and arteriogenesis. Both angiogenesis and arteriogenesis are highly multifactorial processes, and clinical trials aimed at stimulating neovascularization in patients with ischemic disease have been relatively unsuccessful[1,2]. However, in recent years, we, and others, have shown that microRNAs simultaneously regulate multiple facets of neovascularization, acting as a master switch[3,4]. MicroRNAs are endogenous single-stranded RNA molecules of approximately 22 nucleotides long that downregulate expression of their target genes. A single microRNA can influence the expression of hundreds of genes and it has been shown that complementarity of the target gene to the microRNA's seed-sequence, nucleotide +2 to +8 from the 5' end of the microRNA, is crucial for target recognition[5].

The role of microRNAs in vascular disease is well established. They have been shown to influence complex vascular pathological processes, including atherosclerosis, restenosis, aneurysm formation and neovascularization[4,6]. The vasoactive microRNA miR487b is upregulated during chronic hypertension and aneurysm formation in rats[7]. Furthermore, we have shown that miR487b as well as three other microRNAs, all of which are transcribed from a polycistronic microRNA gene cluster located on the long arm of human chromosome 14 (14q32), directly affect blood flow recovery after ischemia in mice[3]. According to TargetScan (www.targetscan.com) however, miR487b has only sixteen conserved putative target genes, while most other microRNAs have hundreds of predicted conserved targets[8]. Despite this, miR487b is still highly conserved in mammals (**Figure 1A**) and broadly regulates neovascularization.

Like all RNAs, microRNAs are subject to modifications, some of which result in sequence editing, which may alter their function. About 90% of all RNA editing events are caused by adenosine-to-inosine (A-to-I) editing[9]. A-to-I editing is catalyzed by the adenosine deaminase acting on RNA family (ADARs) which binds to double-stranded RNA and hydrolytically deaminates adenosine residues changing it to an inosine[10]. Unlike adenosine, inosine preferentially binds to cytidine and is therefore interpreted as guanosine by the cellular machinery. This can have a number of consequences, ranging from destabilization of the RNA molecule by affecting the secondary structure

of the RNA, to changing the sequence of the functional part of the RNA[11]. Dysregulation of A-to-I editing has been shown to contribute to various diseases, including vascular disease[12].

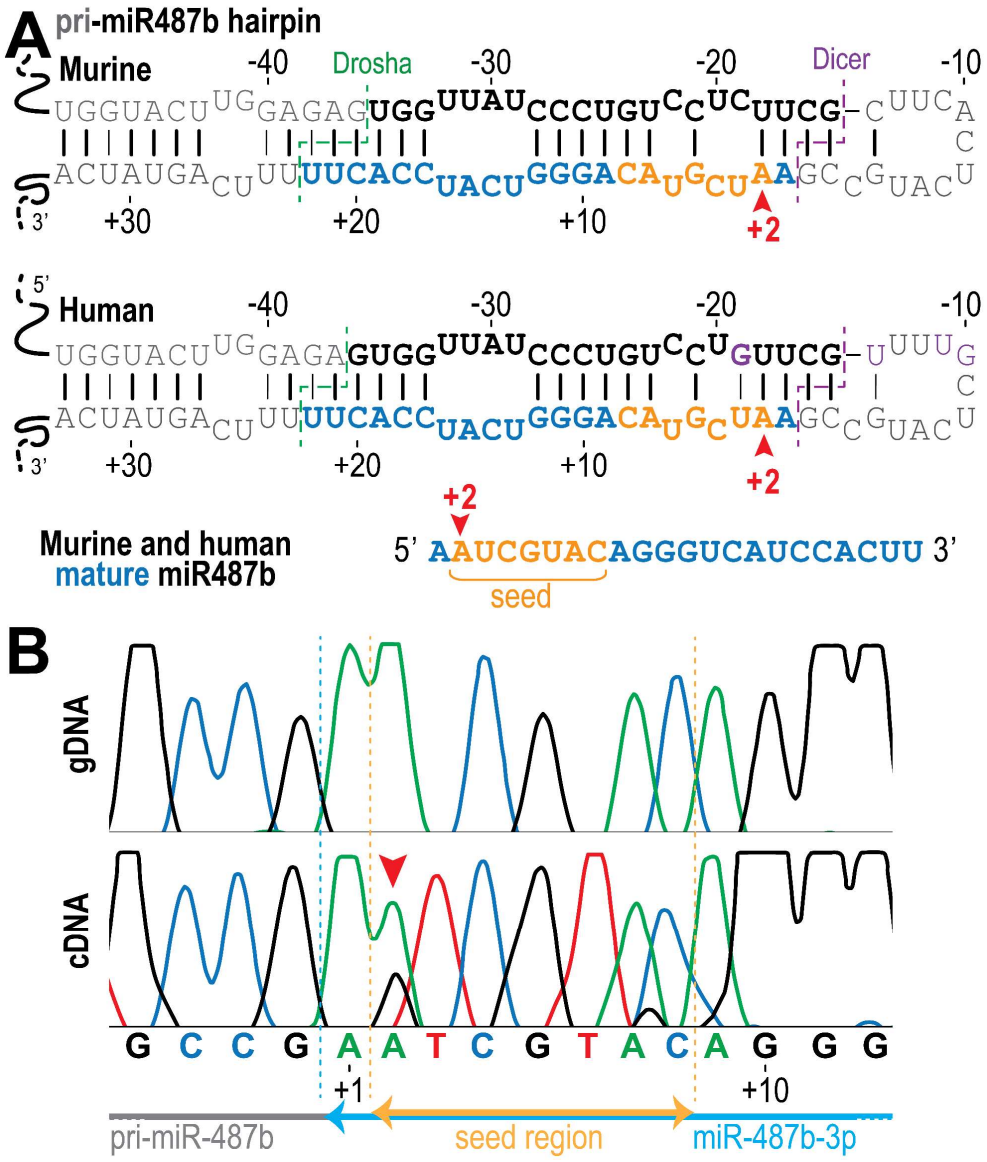


**Figure 1. Primary microRNA 487b and its A-to-I-editing.** (**A**) Schematic overview of primary microRNA 487b (pri-miR487b) hairpin structure and the mature microRNA produced after processing (in blue). Pri-miR487b is highly conserved between the human and murine genome and mature miR487b is fully conserved. Unconserved nucleotides are highlighted in purple, the seed sequence miR487b is highlighted in yellow. Nucleotide numbering is relative to the start of mature miR487b, counted as +1. Dotted lines indicate processing sites. (**B**) Analysis of chromatograms from Sanger sequencing of murine gDNA and muscle tissue cDNA. A-to-I-RNA editing sites are detected when an A-to-G signal is observed in the cDNA sequence chromatogram. Red arrowheads point at the location of editing.

Another common RNA modification is 2'-O-ribose-methylation (2'OMe), which has been shown to be inter-dependent with A-to-I editing[13-15]. 2′OMe is conserved among all major classes of eukaryotic RNA and is guided by small nucleolar RNAs[16]. 2′OMe of an adenosine residue was shown to protect the adenosine from A-to-I editing *in vitro*[13-15].

Primary microRNAs (pri-microRNAs), including several 14q32 pri-microRNAs[17,18], can be A-to-I-edited by ADARs[11]. Editing of a pri-microRNA can influence microRNA maturation, but more interestingly, editing of the seed-sequence can lead to microRNA re-direction and the subsequent recognition of an altered set of target genes, or 'targetome'. This type of editing has been shown to have far-reaching consequences on biological processes. For example, unedited mature 14q32 miR376a* was shown to promote invasive growth of glioblastoma cells, whereas edited mature miR376a* suppressed this phenotype[19]. Furthermore, retargeting of miR376a through editing of the seed-sequence was shown to play a role in uric acid regulation in select brain tissues[20]. So far however, no occurrences of microRNA editing during vascular remodeling have been reported.

Given the narrow range of predicted miR487b target genes mentioned above, we hypothesized that miR487b undergoes A-to-I editing under ischemic conditions. We show here that the first nucleotide of the seed-sequence of pri-miR487b is indeed subject to both A-to-I editing and to 2′OMe in mice and in human primary vascular cells. Using the hindlimb ischemia (HLI) model, we also show that the rate of miR487b A-to-I editing, as well as methylation, is increased under ischemic conditions. The resulting edited mature miR487b has a unique targetome and acts as a pro-angiogenic microRNA.

## METHODS

The data that support the findings of this study are available from the corresponding author upon reasonable request.

Terminology for miR487b and its modified forms are summarized in the **Table**.

**Table: MicroRNA 487b stages and modification terminology**

| Full-length terminology | Symbol/suffix |
|---|---|
| Primary microRNA 487b transcript | pri-miR487b |
| Precursor microRNA 487b | pre-miR487b |
| Mature microRNA 487b | miR487b |
| Unedited microRNA version | miR487b-WT |
| Inosine at +2 microRNA 487b position due to A-to-I editing | miR487b-ED |
| 2'OMe of Adenosine at +2 miR487b position | 2'OMeA |
| Estimated 2'-O-ribose-Methylated Fraction at the +2 miR487b position | EMF |



*Hindlimb Ischemia Model*

Unilateral HLI was induced in C57Bl/6 mice by electrocoagulation of the left femoral artery proximal to the superficial epigastric arteries. Mice were sacrificed by cervical dislocation and the adductor and gastrocnemius muscles were excised en bloc and snap-frozen on dry ice before (T0) and at 1, 3 and 7 days (T1, T3 and T7 respectively) after induction of HLI.

*MiR487b A-to-I editing*

To identify and quantify pri-miR487b editing we performed complement DNA (cDNA) sequencing and total pri-miR487b PCR amplification from cDNA followed by selective digestion of only unedited miR487b using PfeI restriction enzyme (Thermo Scientific). Individual TaqMan miR assays (Applied Biosystems) were used to quantify 'wildtype' miR487b (miR487b-WT) and edited miR487b (miR487b-ED), using a standard kit and a custom kit (targeting 'A**G**UCGUACAGGGUCAUCCACU'), respectively (**Supplemental Figure I**).

*RTL-Q*

To identify and quantify 2'OMe of miR487b, we performed Reverse Transcription at Low deoxyribonucleoside triphosphate followed by Quantitative PCR (RTL-Q), a modification to the RTL-P method, described by Dong *et al*[21] (**Supplemental Figure II**).

*Angiogenesis assays*

Selective miRNA overexpression achieved in cultured primary human vascular cells and in *ex vivo* aortic segments by adding synthetic pre-miR487b-WT or pre-miR487b-ED to culture medium and comparing it to a control pre-miRNA. *In vitro* scratch-wound healing assays and *ex vivo* mouse aortic ring assays were performed as described previously[3,22].

A detailed description of methods and associated references can be found in the **Supplemental Materials**.

## RESULTS

*Discovery of in vivo A-to-I editing of the seed-sequence of pri-miR487b*

To identify editing sites in pri-miR487b, we used Sanger sequencing. cDNA chromatograms of pri-miR487 consistently contained a secondary guanine peak which was absent in chromatograms obtained from genomic DNA (gDNA), indicating the occurrence of A-to-I editing (**Figure 1B**). A-to-I editing occurs on the second nucleotide of the mature miR487b sequence, which is the first nucleotide of the microRNA's seed sequence, changing the seed from 5'-AUCGUAC-3' to 5'-IUCGUAC-3' (**Figure 1A**).

*Validation and quantification of pri-miR487b editing in muscle tissues*

Pri-miR487b contains a digestion site for PfeI, which is abolished by A-to-I editing. PfeI's specificity and efficiency was confirmed by digestion of amplified synthetic DNA of wildtype and edited pri-miR487b (**Figure 2A**).

Next we investigated pri-miR487b editing during different stages of vascular remodelling. Amplified cDNA from gastrocnemius and adductor muscle tissues before (T0) and at 1, 3 and 7 days (T1, T3 and T7 respectively) after hindlimb ischemia (HLI) were digested using PfeI. Even after more than ten times over-digestion, an uncut band remained visible in all samples, confirming the occurrence of A-to-I editing (**Figure 2B**).

In the ischemic gastrocnemius muscle, the percentage of edited pri-miR487b increased by almost 2-fold one day after surgery (T0=6.7±0.4% vs T1=11.7±1.6%, $P$=0.02), but was decreased at 3 and 7 days after surgery (5.0±0.4% and 3.8±0.1%; $P$=0.04 and $P$=0.0005 vs T0, respectively; **Figure 2C**).

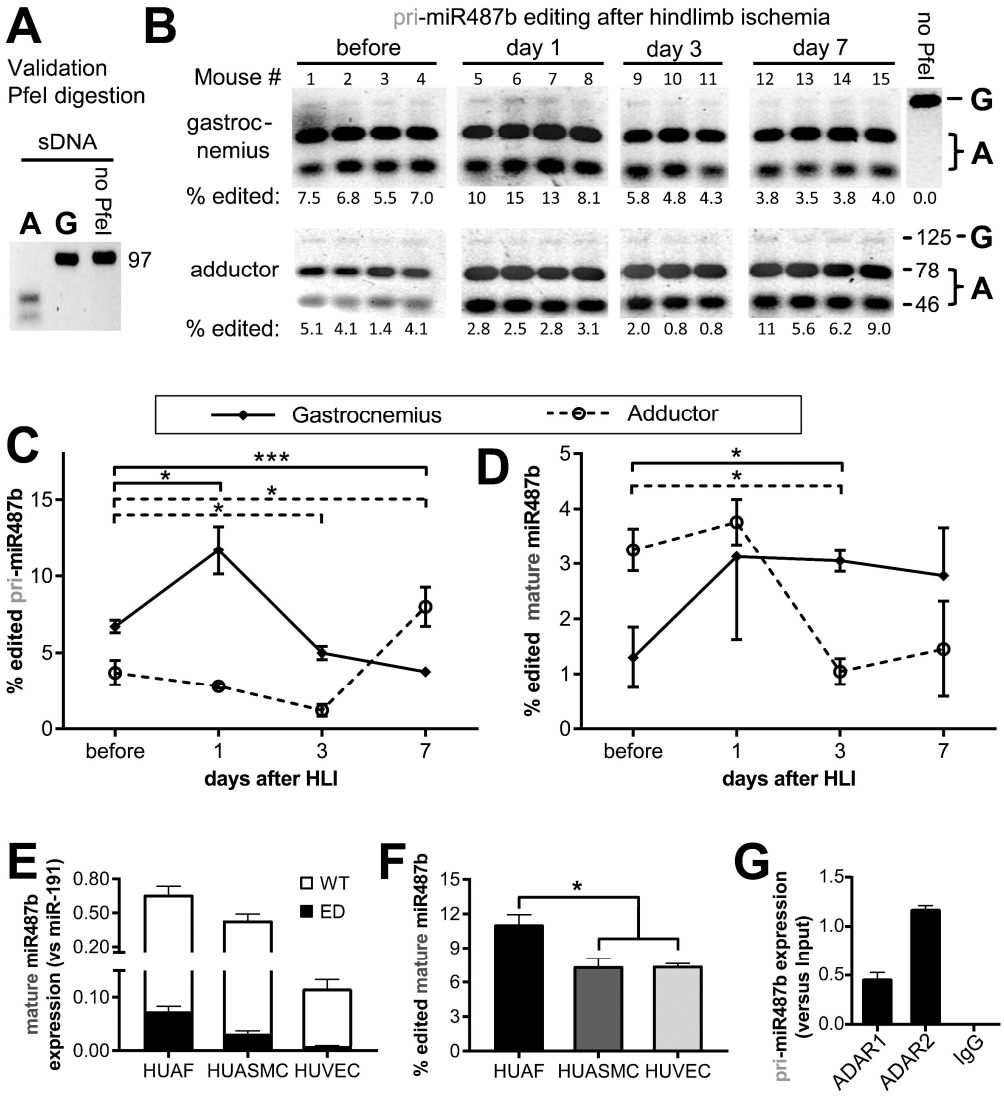


**Figure 2. Validation and quantification of primary and mature miR487b A-to-I-editing in murine muscle tissues and primary human cells.** Specific miR487b-WT digestion of PCR amplified pri-miR487b from (**A**) synthetic DNA (sDNA) and (**B**) cDNA from gastrocnemius and adductor muscle before and after hindlimb ischemia (HLI) by restriction enzyme PfeI. Each lane represents the digestion of the amplified cDNA of one mouse. The percent edited pri-miR487b was objectively calculated by expressing the intensity of the uncut band (G) as a percentage of combined intensity of both cut (A) and uncut (G) bands using computer assisted densitometric analysis. (**C**) Graphical representation of percent edited pri-miR487b. (**D**) Quantification of percent edited mature miR487b in the ischemic murine muscles by rt/qPCR. Per group, murine muscle tissues of 3 (T3 & T7) or 4 (before & T1) were used. (**E**) Relative expression of mature miR487b-WT (green) and miR487b-ED (red) in cDNA from human umbilical arterial fibroblasts (HUAFs), human umbilical arterial smooth muscle cells (HUASMCs) and human umbilical venous endothelial cells (HUVECs) cDNA quantified by rt/qPCR (n=3 or 4). (**F**) Percentage mature miR487b editing calculated from data presented in (**E**). (**A-F**) Data are presented as mean ±SEM. **P*<0.05, ***P*<0.01, ****P*<0.001; by two-sided Student's *t*-test. (**G**) RNA immunoprecipitation on HUAF cell lysate with antibodies for ADAR1, ADAR2 or negative control rabbit IgG followed by RNA isolation and rt/qPCR on precursor miR487b transcript. Data are normalized against 10% input and presented with SEM of technical triplicate.

In the adductor muscle however, the percentage of edited pri-miR487b was unchanged at T1 (2.8±0.1%) compared to T0 (3.7 ±0.8%, *P*=0.3), but decreased at T3 (1.21±0.4%, *P*=0.05 vs T0). At T7, percentage of edited pri-miR487b was increased to 8.0±1.3% (*P*=0.03 vs T0) (**Figure 2C**).

*Mature miR487b editing in muscle tissue and human primary vascular cells*

Next we determined if edited pri-miR487b is processed into edited mature miR487b (miR487b-ED). We used a custom TaqMan rt/qPCR kit to quantify mature miR487b-ED. We found that the edited pri-microRNA is indeed processed, in part, to form a mature microRNA, with percentages of edited miR487b ranging from 1 to 4% of the total mature miR487b in both ischemic gastrocnemius and adductor muscles (**Figure 2D**). The resulting mature microRNA, miR487b-ED, is an entirely new microRNA, with a unique seed and mature microRNA sequence according to miRbase (www.miRbase.com).

Percent mature miR487b-ED in gastrocnemius was low before surgery but increased by more than 2-fold afterward (T0=1.3±0.5% and T3=3.1±0.2%, *P*=0.02). Percent mature miR487b-ED in the adductor muscle however, followed an opposite trend, as percentage editing decreased from 3.3±0.4% at T0 to 1.0±0.2% at T3 (*P*=0.05 vs T0) (**Figure 2D**). Observed changes in percentage miR487b-ED after HLI are predominantly caused by changes in amount of miR487b-ED, rather than by fluctuations in 'wildtype' miR487b (miR487b-WT) expression (**Supplemental Figure III**).

To exclude the possibility that the influx of circulating bone marrow derived cells expressing miR487b-ED could have caused these effects, we measured miR487b in the cDNA of murine bone marrow. Neither miR487b-WT, nor miR487b-ED were expressed in the bone marrow (data not shown).

Editing of human pri-miR487 and mature miR487b at the same position was confirmed in human umbilical artery fibroblasts (HUAFs). In cultured HUAFs, both pri-miR487b and miR487b were found to be edited by approximately 11% (**Supplemental Figure IV A&B** and **Figure 2F**). RNA binding protein immunoprecipitation (RIP) performed on HUAF lysate showed pri-miR487b enrichment in both the ADAR1 and ADAR2 pulldown fractions when compared to the

negative control IgG pulldown, confirming complex formation of ADAR enzymes with pri-miR487b (**Figure 2G**).

Mature miR487b-WT and miR487b-ED expression were also measured in human umbilical artery smooth muscle cells (HUASMCs) and human umbilical vein endothelial cells (HUVECs). We found that fibroblasts had the highest expression of total pri-miR487b and total mature miR487b, as was expected from previous studies[7]. Expression was 5-fold lower in endothelial cells (**Figure 2E** and **Supplemental Figure IV C**). With approximately 7.5% mature miR487b-ED in both HUASMCs and HUVECs, percentage mature miR487b editing was also highest in HUAFs (11%; **Figure 2F**; *P*=0.02 and *P*=0.01 vs HUASMCs and HUVECs respectively). Consistent with this finding, expression of *ADAR1* and especially *ADAR2* appeared higher in HUAFs compared to HUASMCs and HUVECs (**Supplemental Figure IV E&F**).



*2'-O-ribose-methylation of the 2+ adenosine in pri-miR487b*

Besides A-to-I editing, RNA molecules are frequently subject to 2′OMe. As it has been shown that 2′OMe of an adenosine residue in mRNA protects it from A-to-I editing *in vitro*[13-15], we hypothesized that pri-miR487b can be 2'-O-methylated by the methyltransferase Fibrillarin. Fibrillarin-IP showed that pri-miR487b is indeed enriched in the Fibrillarin pulldown fraction, compared to negative control IgG pulldown (**Figure 3A**). We then performed Reverse Transcription at Low deoxyribonucleoside triphosphate followed by Quantitative PCR (RTL-Q) to quantify the estimated specific 2'-O-ribose-methylated fraction (EMF) in the gastrocnemius and adductor muscle before and after hindlimb ischemia induction. Interestingly, we found specific 2'OMe (2'OMeA) of pri-miR487b at the exact same adenosine residue that is subject to editing (+2A), in all sample types (**Figure 3C** and **D**), which corresponds with the adenosine position where A-to-I editing occurs. We observed a similar baseline of specific 2'OMe in both adductor and gastrocnemius muscle of approximately 33% EMF before surgery (32.8±14% and 33.6±12% respectively). After femoral artery ligation, the EMF appeared to increase initially in the ischemic gastrocnemius muscle (T1=53.6±12%, *P*=0.27), but decreased again by day 3 and 7 (23±11% and 17±9%, *P*>0.1 and *P*=0.03 vs T1, respectively; **Figure 3C**). In the adductor muscle, the EMF of pri-miR487b also appeared to increase 1 day after surgery to 43.8±11% (*P*=0.55), but on T3

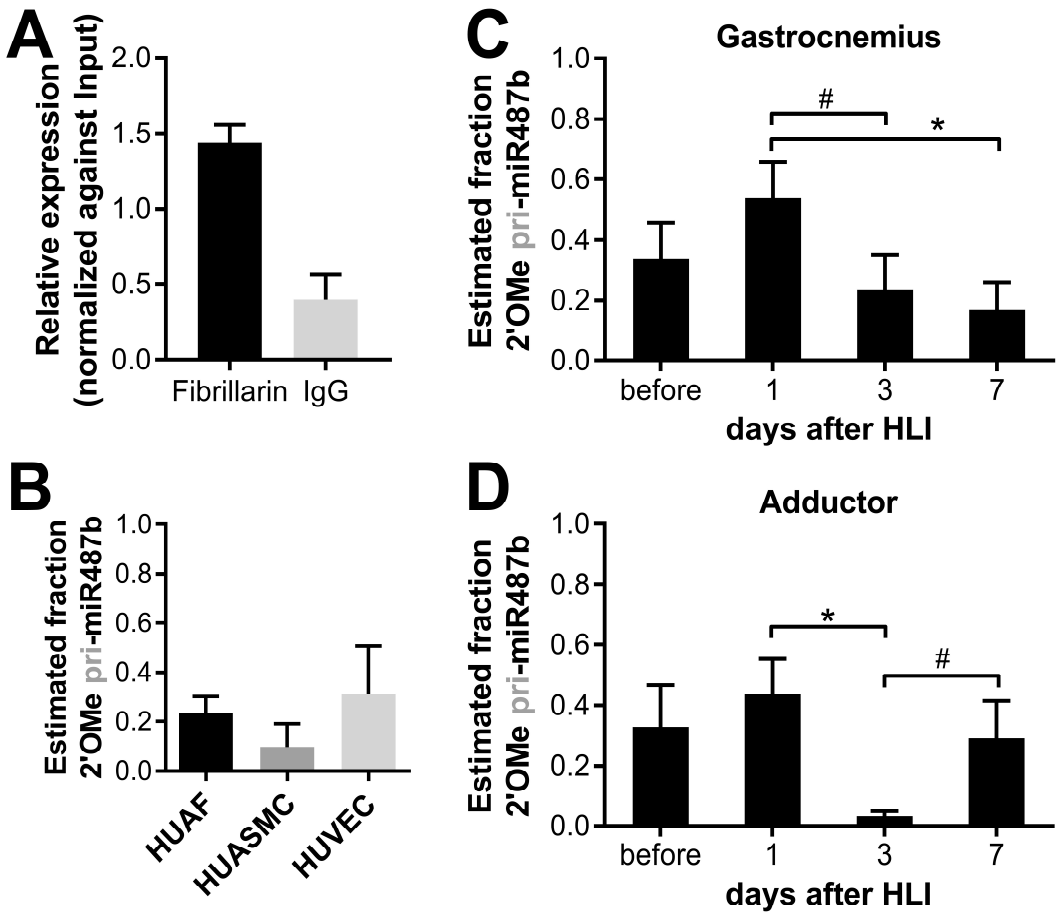


**Figure 3. 2'-O-ribose-methylation of human and murine pri-miR487b at the 2+ adenosine position.** (**A**) Pri-miR487b expression in HUAF lysate samples after immunoprecipitation of Fibrillarin or negative control IgG. Estimated 2'O-ribose-methylated fraction (EMF) of pri-miR487b at the +2 position in (**B**) HUAF, HUASMC and HUVEC; (**C**) Gastrocnemius or (**D**) Adductor RNA isolate as determined by RTL-Q (**Supplemental Figure II**). EMFs are presented as mean ±SEM of 3 or 4 biological replicates (**B**) or at least 3 mice per group (**C** and **D**). **P*<0.05, #*P*<0.1; by two-sided Student's *t*-test.

2'OMe had almost been abolished (EMF of 3.2±1.6%, *P*=0.02 vs T1), to recover again by day 7 (EMF of 29.0±12%, *P*>0.1 vs T3; **Figure 3D**). Therefore specific 2'OMeA of pri-miR487b followed the same, and not the hypothesized inverse, pattern as pri-miR487b A-to-I editing.

2'OMe of the same adenosine residue was confirmed for human pri-miR487b. We observed an EMF of 24±7% in HUAFs, an EMF 9.5±9% of in HUASMC, and an EMF of 31±19% in HUVECs (**Figure 3B**). Relative *Fibrillarin* expression measured in these

different cell types were consistent with these differences in average pri-miR487b methylation (**Supplemental Figure IV D**).

*ADAR1, ADAR2 and Fibrillarin in miR487b expression, editing and methylation*

To gain further insights into miR487b editing and methylation and their potential interplay, *ADAR1*, *ADAR2* and *Fibrillarin* were individually repressed in HUAFs using short interfering RNAs (siRNAs). Knockdown of *ADAR1* or *ADAR2* both resulted in significantly decreased amount of pri-miR487b editing compared to control siRNA (**Figure 4A** and **B**; *P*=0.02 and 0.05 respectively), demonstrating that both ADAR1 and ADAR2 can edit pri-miR487b. This reduction was not observed in percentage mature miR487b editing, indicating that microRNA processing contributes to determine the final levels of mature edited microRNAs (**Figure 4C**).

ADAR1 and ADAR2 are also known to play independent roles in microRNA biogenesis and maturation[23,24]. We found that repression of either *ADAR1* or *ADAR2* caused a 2-fold reduction in total pri-miR487b expression (**Figure 4D**; *P*<0.01 for both), but at mature miR487b level, only miR487b-WT was reduced after *ADAR1* repression (**Figure 4E**; *P*=0.02). Repression of *Fibrillarin* resulted in a 17% decrease in pri-miR487b 2'OMeA relative to control (*P*=0.07), indicating that the methylation of pri-miR487b is indeed Fibrillarin-dependent 2'-O-methylation (**Figure 4F**). Reduced pri-miR487b 2'-O-methylation after *Fibrillarin* knockdown had little effect on miR487b A-to-I editing however, suggesting these pri-miR487b modifications are not directly inter-dependent (**Figure 4B&C**).

Interestingly, specific knockdown of *ADAR1* or *ADAR2* did not only reduce A-to-I editing in both cases, but also significantly increased pri-miR487b 2'OMeA by 1.4-fold compared to control (*P*<0.001 for both). Analysis of *Fibrillarin* expression revealed that knockdown of *ADAR1* or *ADAR2* causes a 3-fold increase in *Fibrillarin* expression (**Figure 4G**, *P*<0.001 and *P*=0.03 vs control respectively). Correspondingly, siRNA-mediated *Fibrillarin* knockdown also caused significant increases in *ADAR1* and *ADAR2* expression (**Figure 4G**, *P*=0.01 vs control for both). Taken together, these findings suggest that pri-miR487b 2'-O-methylation and A-to-I editing are not directly interdependent, but instead that there is a direct inverse correlation between *ADAR1* and *ADAR2* expression on the one hand and *Fibrillarin* expression on the other.

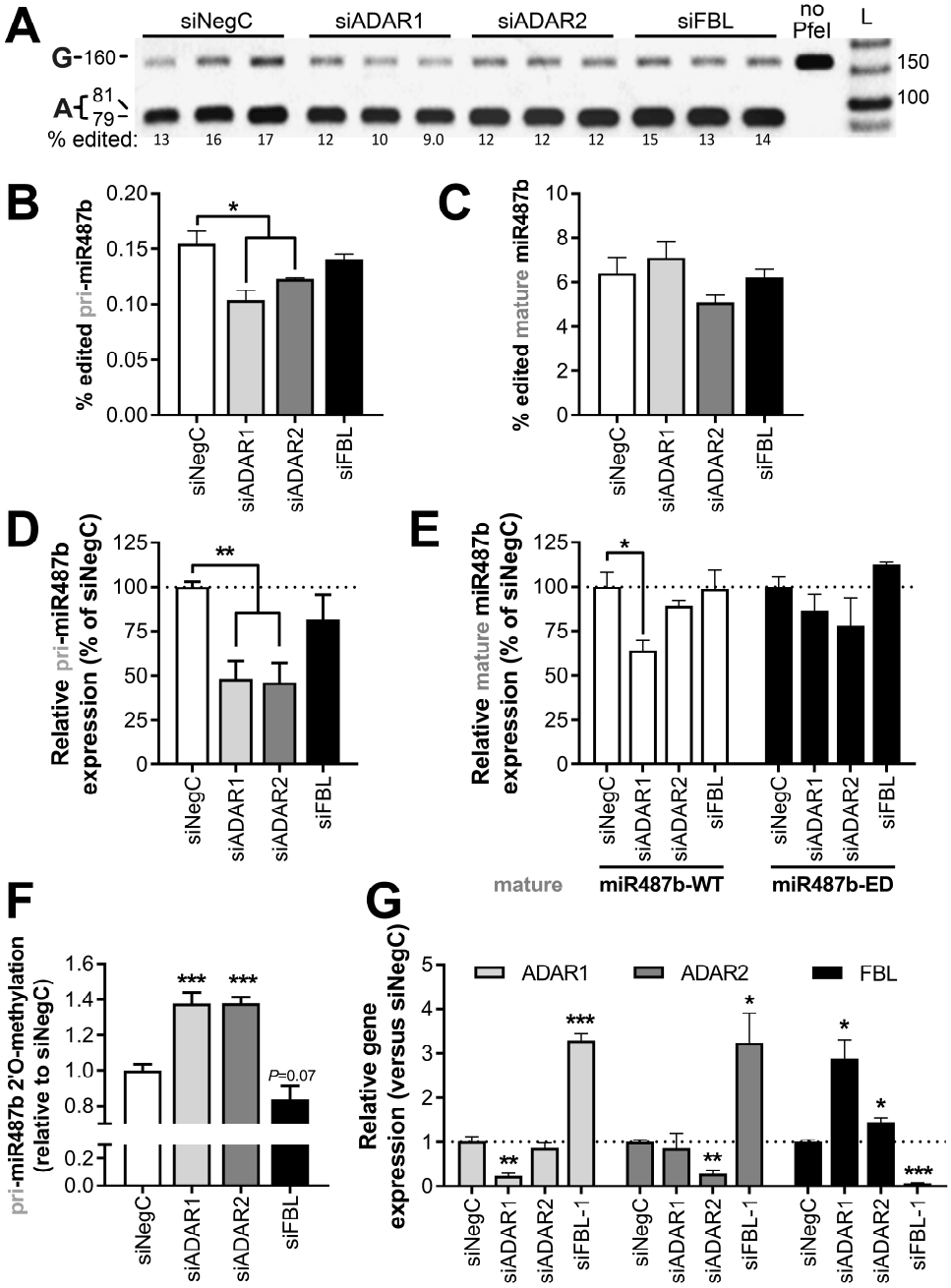


**Figure 4. Role of ADAR1, ADAR2 and Fibrillarin in miR487b expression, editing and methylation.** HUAFs were transfected with a negative control, *ADAR1*-targeted, *ADAR2*-targeted or *Fibrillarin*-targeted siRNA (siNegC, siADAR1, siADAR2 and siFBL respectively). The cDNA obtained was used to analyze all subsequent effects on miR487b expression, editing and 2'-O-ribose methylation analyses, performed as before. (A) PfeI digestion of PCR amplified pri-miR487b from siRNA treated cDNA and (B) quantification of percentage pri-miR487b editing. (C-E) Quantification of percentage mature miR487b editing (C), total pri-miR487b expression (D) and relative mature miR487b (E) expression by rt/qPCR. (F) EMF of pri-miR487b at the +2 position determined by RTL-Q. (G) Analysis of *ADAR1*, *ADAR2* and *Fibrillarin* expression by rt/qPCR. All data were expressed as percent expression of siNegC and presented as mean ±SEM (n=3 per treatment). **P*<0.05, ***P*<0.01, ****P*<0.001; versus siNegC by two-sided Student's *t*-test.

*Comparison of putative targets of edited and unedited miR487b*

Changes in the seed-sequence of a microRNA may shift its targetome. Using Diana-MR-microT software[25,26], we found that there was only an approximately 15% overlap between the miR487b-WT and miR487b-ED targetomes (**Figure 5A**). The overlapping target genes all contained separate binding sites for both miR487b-WT and miR487b-ED in their 3'UTR.

Pathway enrichment analysis using the PANTHER algorithm revealed enrichment for CCKR signaling, the Ras pathway, the PDGF signaling pathway and insulin/IGF associated pathways (*P*=0.004, 0.023, 0.036 and 0.049, respectively) within the miR487b-WT's murine targetome, but none for its human targetome (**Figure 5A** and **Supplemental Table IIIa**). The targetome of miR487b-ED on the other hand contained robust enrichment for several pathways in both man and mouse. Specifically, miR487b-ED's murine targetome contained enrichment for the Wnt signaling pathway and the Cadherin signaling pathway (both *P*>0.00001). Furthermore, within miR487b-ED's human targetome Wnt signaling was also enriched (*P*=0.004) in addition to the Angiogenesis pathway, the PDGF signaling pathway and insulin/IGF associated pathways (*P*=0.004, 0.015 and 0.041, respectively). Numerous publications could be found linking each enriched pathway to neovascularization, ischemia and vascular disease for all enriched pathways with the exception of the CCKR signaling (**Supplemental Table IIIb**).

*Validation of target shift induced by miR487b seed sequence editing*

Next we set out to test whether the single nucleotide change in the seed sequence of miR487b indeed causes a shift in target site selection. We performed dual luciferase reporter gene assays using endogenous and mutated putative miR487b binding sequences from IRS1 and BMP1.

The 3'UTR of IRS1 contains one predicted binding site for miR487b-WT and one predicted binding site for miR487b-ED (**Supplemental Figure V**). Dual luciferase reporter gene assays showed that miR487b-WT caused an 11±6% inhibition of luciferase activity of the endogenous IRS1 sequence (*P*=0.3; **Figure 5B**), which is similar to previously published results[7]. MiR487b-ED, on the other hand, significantly inhibited luciferase activity by 54±2% (*P*<0.0001) through binding to endogenous IRS1

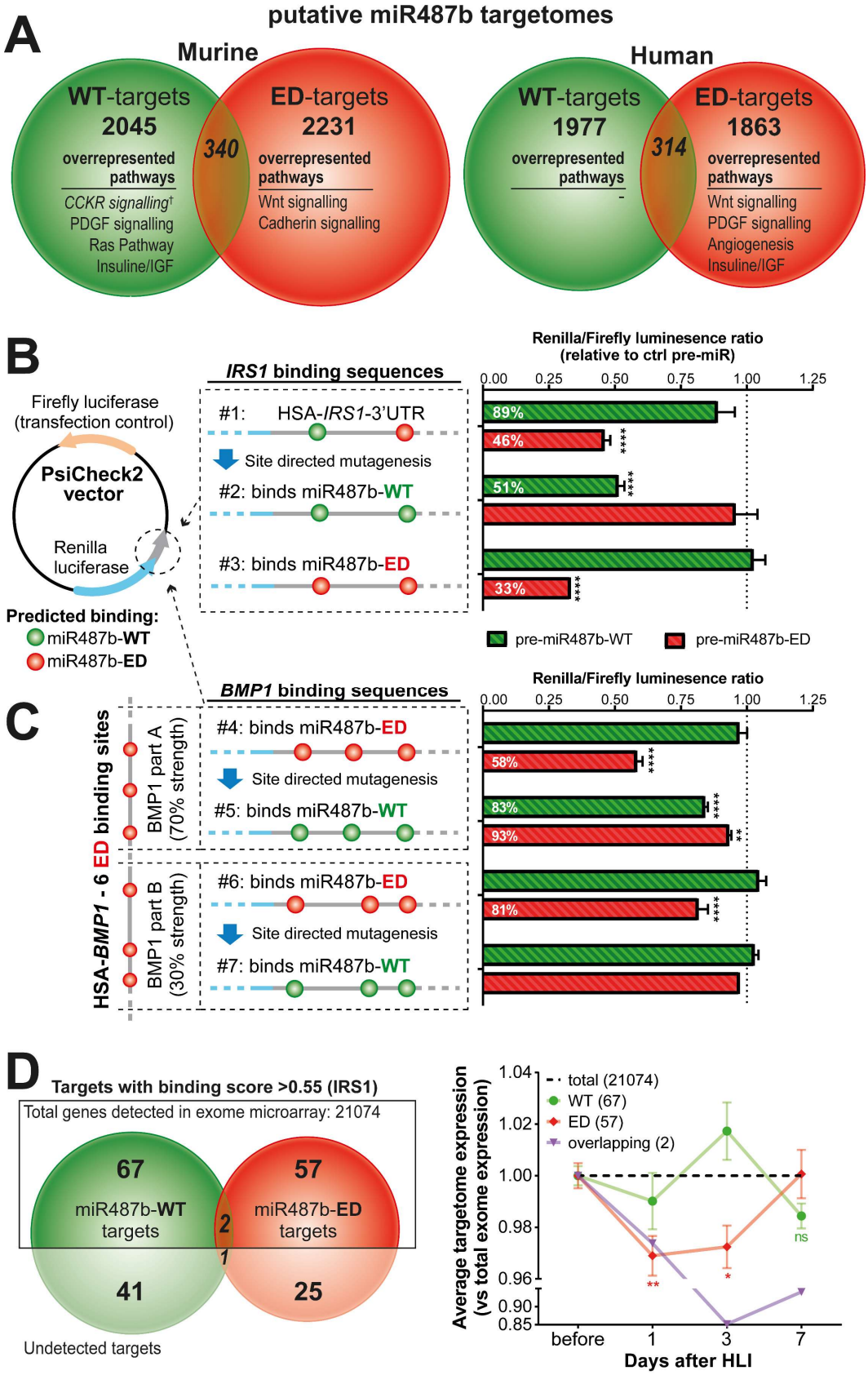


**Figure 5. MiR487b-WT and miR487b-ED targetome predictions, binding shift validation and *in vivo* targetome expression.** (**A**) Venn diagram of *in silico* predicted target genes of miR487b-WT (green) and miR487b-ED (red) in the murine and human genome. Within each putative targetome, significantly enriched pathways were displayed

3'UTR. When the first putative binding site of endogenous IRS1 3'UTR was mutated so that both sites became putative target sites for miR487b-ED, miR487b-WT had no effect when compared to the control pre-miR (*P*=0.95), while knockdown by miR487b-ED increased to 67±2% compared to the control (*P*<0.0001; **Figure 5B**). Conversely, when the second putative binding site was mutated instead, so that both sites became putative target sites for the miR487b-WT, miR487b-WT inhibited luciferase activity by 49±2% (*P*<0.0001), while miR487b-ED had no effect (*P*=0.9).

BMP1 is predicted to have six separate binding sites for miR487b-ED (**Supplemental Figure VI**). Binding of miR487b to *BMP1*'s first three putative binding sites (part A) was assessed separately from binding to its last three target sites (part B), which confer an estimated 70% and 30% of the combined binding strength, respectively. Luciferase activity clearly reflected the difference in predicted binding strength, with miR487b-ED repressing luciferase activity of BMP1 part A by 42±2% and

◀ **Figure 5 continued:** (see **Supplemental Table III A**). †Of all enriched pathways, only CCKR signalling was not linked to neovascularization or ischemia (**Supplemental Table III B**). Schematic diagram of the PsiCheck2 vector constructs with endogenous and mutated *IRS1* (**B**) and *BMP1* (**C**) binding sequences inserted used in dual luciferase reporter gene assays. Human *IRS1* 3'UTR contains one putative binding sites for both miR487b-WT and miR487b-ED, whereas human *BMP1* contains six putative miR487b-ED binding sites. One luciferase reporter construct was created with both *IRS1* binding sites (#1) and another with *BMP1*'s first three putative binding sites (part A, #4) and one more with the last three binding sites within *BMP1* (part B, #6). Next, a single nucleotide within endogenous binding sequences was mutated to create additional reporter constructs with either only binding sites for miR487b-ED (#2) or for miR487b-WT (#3, #5 & #7) to compare wildtype versus edited miR487b binding in an identical context. Constructs were individually co-transfected into HeLa cells with either a synthetic pre-miR that produces miR487b-WT, a miR487b-ED mimic, a control miRNA or vehicle. The ratios of measured luminescence were corrected for differences in baseline vector luminescence observed in vehicle treated group and expressed as fraction of control luminescence (dotted line). (**B**&**C**) Data are presented as mean ±SEM and represent data obtained from 3 independent experiments with 4 wells per vector. ***P*<0.01, *****P*<0.0001 compared with scrambled control. (**D**) Schematic overview of putative target genes as in **Figure 4**, after applying lowest luciferase binding score (0.55 for miR487b-WT binding to IRS1-3'UTR) as threshold (left panel). This time, targetomes were split up into targets genes that were detected above array background levels (top part) and those that weren't (bottom) in whole-genome expression microArray performed on mRNA of total adductor muscle mRNA of the same mice used in previous HLI experiments. The right panel shows the mean fold targetome expression change of miR487b-WT and miR487b-ED (green and red respectively) after HLI. Targetome expression was normalized to expression of total number of genes detected and presented as mean ±SEM of at least 3 different mice per timepoint. **P*<0.05, ***P*<0.01; versus control whole-genome expression by two-sided Student's *t*-test.

only 19±2% for part B (**Figure 5C**, *P*<0.0001 for both). miR487b-WT on the other hand had no effect on luciferase activity of either BMP1 constructs containing endogenous miR487b-ED binding sites. Next a single nucleotide was mutated in each binding site, so that all sites within the BMP1 3'UTR sequences became putative target sites for miR487b-WT instead. MiR487b-WT repressed luciferase activity of the mutated BMP1 part A by 17±1% (*P*<0.0001), but had no effect on the weaker sites of mutated BMP1 part B (*P*=1.0). miR487b-ED had no effect on the mutated BMP1 part B either, but was still able to cause a mild repression of mutated BMP1 part A luciferase activity (7±1%; *P*<0.01).

*Specific regulation of endogenous targets by miR487b-WT and miR487b-ED*

To confirm endogenous target regulation by miR487b-WT and miR487b-ED is also selective, we overexpressed miR487b-WT or miR487b-ED in HUAFs and HUVECs and measured the expression of a subset of putative target genes. Expression of miR487b-WT targets *DNAJC9, B3GALNT2* and *MAP2K4* were repressed after miR487b-WT overexpression compared to control in both HUAFs and HUVECs, but not after miR487b-ED overexpression (**Figure 6A-C**). *RPS6KB1* and *BMP1* on the other hand only contain miR487b-ED binding sites and were repressed after miR487b-ED overexpression in both HUAFs and HUVECs, but not after miR487b-WT overexpression (**Figure 6D&E**). Furthermore, endogenous *IRS1*, with one binding site for miR487b and miR487b-ED each, was repressed after overexpression of either miR487b-WT and miR487b-ED, again in both HUAFs and HUVECs (**Figure 6F**). Taken together, these finding show that editing of miR487b does change binding site selection and that miR487b-WT and miR487b-ED regulate different targetomes.

*Expression of miR487b-WT and miR487b-ED targetomes in the adductor muscle*

A microRNA influences complex biological processes by fine-tuning the expression of its broad targetome rather than causing strong downregulation of single genes[27]. We examined *miR487b-WT and miR487b-ED* targetome gene expression by using an existing dataset of whole-genome expression microArray performed on total adductor muscle mRNA of mice after induction of HLI[28]. Average expression of the 1353 detected genes within targetome for miR487b-WT was repressed at T1 by 0.8±0.3% (*P*=0.004) and at T7 by 0.6±0.3% (*P*=0.03) compared to total detectable genome

expression (**Supplemental Figure VII**). For the miR487b-ED targetome however, average expression of its 1521 detectable genes was repressed at all timepoints after HLI, with 0.6±0.2% (*P*=0.04) repression at T1 and 0.7±0.2% at T3 and 0.9±0.1% at T7 (*P*=0.003 and *P*=0.0005, respectively). Averaged expression of the 232 overlapping target genes of *miR487b-WT and miR487b-ED* was also repressed at all timepoints after surgery, but approximately twice as strongly as that of the total edited targetome (T1=1.4±0.4%, T3=1.8±0.5% and T7=1.6±0.6%, *P*=0.04, *P*=0.0005 and *P*=0.008 vs total, respectively).

Next we filtered putative target genes based on a Diana binding score similar or better than that of the endogenous binding sites that were confirmed using luciferase assays (Diana binding score>0.55). A higher binding score indicates an increased likelihood or efficiency of target gene suppression by the microRNA. Expression patterns of the restricted miR487b-WT targetome followed a similar pattern to its unrestricted one, but did not differ significantly any more from total genome expression (**Figure 5D**). Binding score restriction of the miR487b-ED targetome on the other hand, only resulted in loss of average expression knockdown at T7, while increasing repression by more than 4-fold at T1 to 3.1±0.8% (*P*=0.02) and by 3-fold at T3 to 2.8±0.7% (*P*=0.009).

*Causal involvement of miR487b-ED and not miR487b-WT in neovascularization in vitro*

To examine the effects of miR487b-ED, we overexpressed miR487b-WT or miR487b-ED in mouse aortic segment *ex vivo* (**Supplemental Figure VIII A&B**). We observed an almost 3-fold increase in the number of neovessels formed in the miR487b-ED treated aortic segments compared to control, whereas miR487b-WT over-expression did not increase sprout-formation (**Figure 7A**; *P*=0.002 and 0.25 respectively). Cell type specific triple stainings of aortic segments confirmed that the sprouting neovessels are lined with endothelial cells, as described previously[22]. The endothelial cells were surrounded by a highly organized layer of fibroblasts, underlining the importance of fibroblasts in neovascularization. Smooth muscle cells were less abundant and more disorganized in all three groups, miR487b-WT, miR-487b-ED and control (**Figure 7B**).

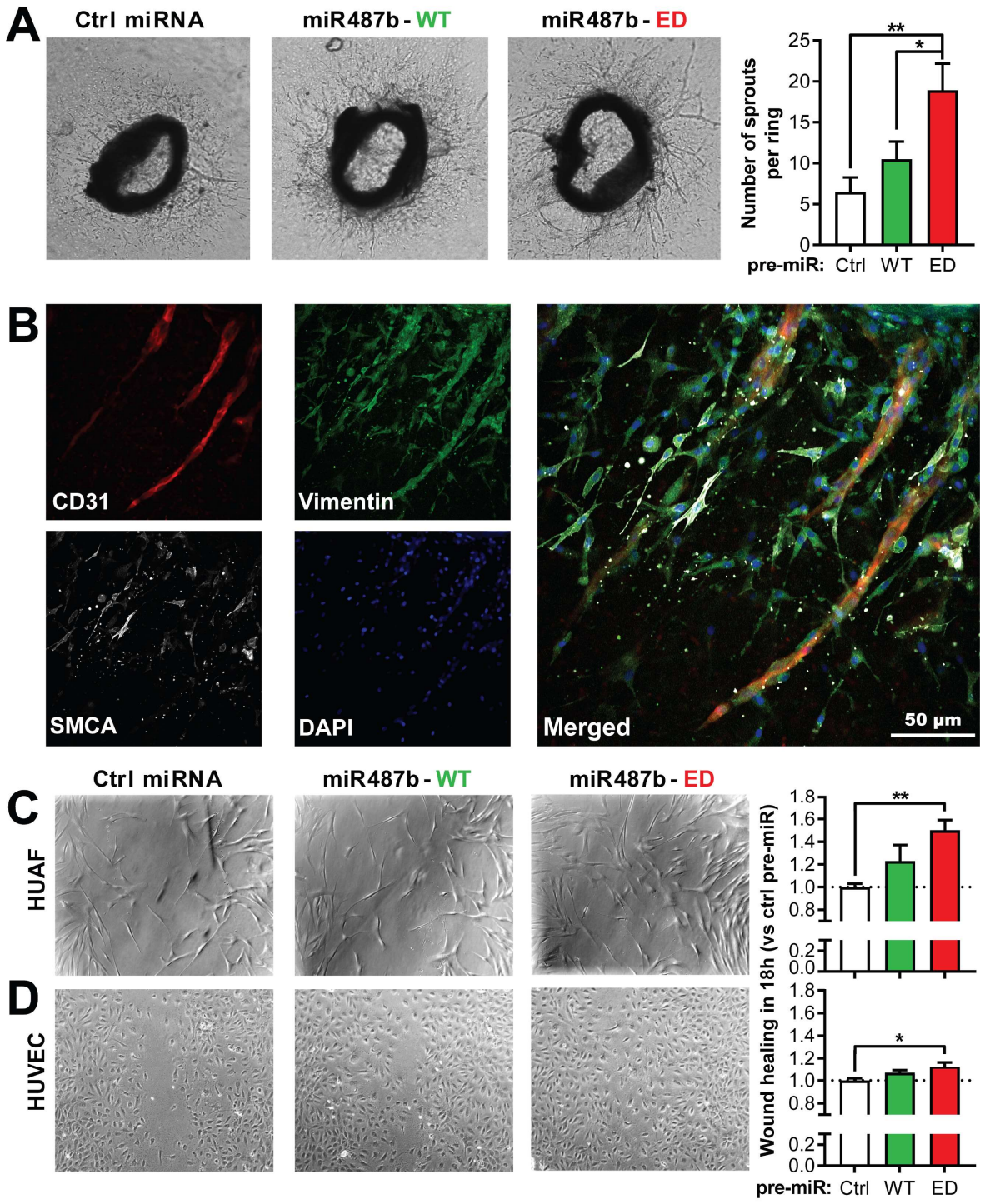


**Figure 7. Functional effects of miR487b-WT or miR487b-ED on neovascularization assays.** (**A**) Representative images (left) and quantification of neovessel sprouts (right) after overexpression of miR487b-WT or miR487b-ED in an *ex vivo* aortic ring assay. Data is presented as mean ±SEM of 15 aortic segments per treatment, which were cut from aortas of 6 different mice. (**B**) Representative example of Z-stacks confocal images of complex aortic ring neovessel sprouts fluorescently stained with cell specific markers. CD31 (red) stains endothelial cells; Vimentin (green) indicates fibroblasts; α-SMA (white) indicates smooth muscle cells; DAPI-stained nuclei (blue). Effects of miR487b-WT or miR487b-ED overexpression on scratch wound healing of HUAFs (**C**) or HUVECs (**D**). Representative images are shown on the left, while quantification is shown on the right. **P*<0.05, ***P*<0.01; versus pre-Ctrl by two-sided Student's *t*-test.

Next, we investigated the effects of miR487b-WT or miR487b-ED overexpression on cell migration, using a scratch-wound healing assay in both HUAFs and HUVECs. Overexpression of the microRNAs in both HUAFs and HUVECs is shown in **Supplemental Figure VIII** C-E. Treatment with miR487b-ED significantly increased scratch-wound closure in HUAFs by 50±9% and in HUVECs by 13±4% compared to control (**Figure 7C&D**, *P*=0.006 and 0.04 respectively), while miR487b-WT treatment did not (*P*=0.2 and 0.11 for HUAF and HUVECs respectively).

## DISCUSSION



In this study we show that the seed-sequence of miR487b is subject to A-to-I editing by ADARs both in mice and in human primary cells, which results in a novel microRNA, miR487b-ED. The rate of miR487b editing is increased during active neovascularization after ischemia. Additionally, we found Fibrillarin-dependent 2'-O-ribose-methylation of miR487b at the same adenosine-residue that is subject to A-to-I editing in murine muscle tissue and human primary cells. While post-ischemic miR487b editing and 2'OMe patterns are similar, *in vitro* mechanistic studies suggest an inverse-correlation between expression of the ADAR proteins on the one hand and Fibrillarin on the other. *In vitro* luciferase reporter gene assays and target validation experiments demonstrated that miR487b editing results in a complete shift in target site selection. In contrast to miR487b-WT, the putative targetome of miR487b-ED is actively repressed during effective neovascularization after ischemia and is enriched for neovascularization-associated pathways. MicroRNA overexpression experiments demonstrated that miR487b-ED causes a 2-fold increase in neovascularization compared to miR487b-WT in an *ex vivo* aortic ring sprouting assay and also increases wound healing in both human vascular endothelial cells and fibroblasts.

To our knowledge, we are the first to demonstrate A-to-I editing of the angiomiR miR487b. Furthermore, our study provides the first evidence of altered microRNA editing during vascular remodeling and ischemia in general. In a recent study by Nigita *et al*[29], the authors detected similar percentages of mature microRNA-seed editing of 7 microRNAs in small-RNAseq datasets of breast adenocarcinoma cell line MCF-7 cultured under normoxic and a time-course of hypoxic conditions. For most of these microRNAs, a trend of increasing microRNA-seed editing with increasing hypoxia was

observed, however the study's setup lacked power to establish a significant correlation. Our study used a hypothesis-driven methodology, opposed to a discovery-based method of RNAseq, which allowed us to focus on a specific region. Because of this, we were able to show statistically significant changes, not only in mature microRNA, but also in primary microRNA editing.

The positive trend of microRNA-seed editing with increasing hypoxia found by Nigita *et al* corresponds to our findings, where we demonstrate increased mature miR487b editing in the strongly ischemic gastrocnemius muscle, which displays angiogenesis after femoral artery ligation. In contrast, we observed decreased miR487b editing in the adductor muscle. This can most likely be attributed to the fact that the adductor experiences predominantly increased shear stress instead of ischemia, causing mainly arteriogenesis instead of angiogenesis after femoral artery ligation[30,31]. We observed that baseline percentages of pri-miR487b and mature miR487b editing also differed between both muscles. This is consistent with previous findings showing that levels of both total and site specific A-to-I editing, as well as pri-miRNA maturation, can vary strongly per tissue[17,32-36].

A-to-I editing is directed by the enzymes ADAR1 and ADAR2. We demonstrated that pri-miR487b associates with both ADAR1 and ADAR2 and is also edited by both enzymes. ADARs appear to modify specific adenosines to inosines in short and imperfect dsRNA substrates like pri-microRNAs, however, they do not require strict sequence specificity[11,37,38]. Therefore, it is not directly possible to contribute the increase in miR487b editing after ischemia to either ADAR enzyme. Neither could we observe a correlation between *Adar1* or *Adar2* expression and percentage of editing. In the adductor muscle, *Adar1* mRNA levels were increased at day 1, and *Adar2* levels were increased at day 3 after femoral artery ligation (**Supplemental Figure IX**), while observed pri-miR487b editing dropped by 3-fold. It has been shown before that changes in ADAR expression or activity do not always correlate with frequencies of specific editing[39,40]. As a result, additional regulatory mechanisms, potentially including 2'OMe, are thought to modulate editing of specific adenosine residues.

Based on previous *in vitro* findings that 2′OMe of an adenosine in specific mRNAs can protect it from deamination by ADARs[13-15], we hypothesized that the adenosine we showed to undergo editing in pri-miR487b, can also be 2'-O-ribose-methylated. In this

study, we demonstrate that pri-miR487b associates with 2'-O-ribose-methyltransferase Fibrillarin. Using RTL-Q, a modified 2'OMe detection method that allows for quantitative estimation of specific nucleotide 2'OMe, we showed that pri-miR487b is indeed 2'-O-ribose-methylated in murine muscle tissues and in human primary cells at the same adenosine residue that is subject to editing. However, like A-to-I editing, estimated 2'-O-ribose-methylated fraction (EMF) appeared to increase at day 1 after induction of HLI in the gastrocnemius and decreased again by day 3 and 7. Furthermore, in the adductor muscle, EMF of pri-miR487b also followed the same pattern as A-to-I editing, since both decreased from day 1 to day 3 after surgery, only to increase again by day 7. These data suggest a positive correlation between A-to-I editing and 2'OMe rather than the previously reported negative correlation. However, further *in vitro* mechanistic studies showed that a reduced pri-miR487b 2'OMe after *Fibrillarin* knockdown had little effect on pri-miR487b A-to-I editing, suggesting that for the specific case of pri-miR487b, these modifications are not directly inter-dependent. We did uncover an inverse correlation between expression of *ADARs* and *Fibrillarin in vitro;* knockdown of *ADAR1* or *ADAR2* causes a 3-fold increase in *Fibrillarin* expression, and knockdown of *Fibrillarin* results in significant increases in both *ADAR1* and *ADAR2* expression. To our knowledge, this is a novel finding, which may help explain the previously reported inverse correlation between A-to-I editing en 2'O-ribose methylation of RNAs[13-15].

The seed-sequence of miR487b-ED is different from any known microRNA in humans and mice, meaning that because of A-to-I editing, an entirely new microRNA with a novel targetome is created. Through luciferase reporter gene assays and validation of a subset of target genes, we showed that editing of the seed-sequence of miR487b does indeed completely shift its target site selection. In an identical context, miR487b-ED induced stronger luciferase silencing than miR487b-WT binding. Furthermore, we found more active repression of miR487b-ED's targetome in the adductor muscle after HLI, than miR487b-WT, especially when we focus on putative targets with a strong Diana binding score. Unlike for miR487b-WT's targetomes, both human and murine miR487b-ED targetomes were significantly enriched for multiple pathways that are associated with angiogenesis, arteriogenesis and vascular disease. The murine targetome of miR487b-WT did contain enrichment for several

neovascularization-related pathways, as was to be expected based on our previous findings[3,7], but also displayed robust enrichment for CCKR signaling, which is associated with gastrointestinal peptide hormones cholecystokinin and gastrin instead[41]. Surprisingly, no enriched pathways were found within the miR487b-WT's human targetome. The enriched pathways within human and murine miR487b-ED targetomes all contain obvious ties to neovascularization and vascular disease, including Angiogenesis-related signaling and the Insuline/IGF pathway in humans and the Cadherin signaling pathway in mice, in addition to Wnt signalling, for which enrichment appears to be conserved across both species. Interestingly, Wnt signaling has been implicated to promote vascular remodeling and even cardiovascular regeneration[42].

We performed microRNA overexpression experiments in an *ex vivo* aortic ring sprouting assay and an *in vitro* scratch-wound healing assay to examine the functional effects of miR487b-WT and miR487b-ED on angiogenesis. We found that miR487b-ED treatment resulted in an increase in both neovessel formation and scratch wound healing, whereas miR487b-WT did not. These results reflect the stronger enrichment of angiogenesis-associated pathways within the miR487b-ED putative targetome. Combined with miR487b-ED's higher target gene silencing efficacy, our findings suggest that editing of miR487b plays a central role in neovascularisation.

As the expression of edited mature microRNAs is low compared to their unedited counterparts, it is difficult to estimate the clinical significance of A-to-I editing of microRNAs. However, the potential for a clinical relevance is undeniable, as illustrated by the seed-sequence editing of, for example, miR455. Highly metastatic melanoma cells were shown to have reduced ADAR1 levels resulting in reduced miR455 editing, yielding increased inhibition of the CPEB1 gene, a known tumor suppressor gene[43]. Furthermore, overexpression of unedited miR455 was shown to promote tumor growth and lung metastasis, whereas overexpression of edited miR455 suppressed this phenotype. With regards to cardiovascular disease and vascular remodeling, Stellos et al. were the first to demonstrate that A-to-I editing can control gene expression in human atherosclerotic diseases. They showed that editing of the cathepsin S mRNA, which encodes a cysteine protease associated with angiogenesis and atherosclerosis, is increased in plaques from atherosclerotic patients with increased expression as a

result. Interestingly, they also showed that ADAR1 controls HUVEC function and that ADAR1 expression is strongly increased in and around plaques from atherosclerotic patients. While their focus was on the editing of long RNAs with double-stranded regions due to presence of inverted Alu repeats, this study underlines the importance of A-to-I editing in general. We provide new evidence that A-to-I editing also controls the expression of numerous other genes in angiogenesis and ischemia by regulation of microRNA targeting.

In conclusion, we demonstrate that the angiomiR miR487b undergoes A-to-I editing and 2'OMe in the seed-sequence of the microRNA, creating a completely new microRNA unlike that of any known human or murine microRNA. The amount of editing is significantly increased after ischemia in mice. Editing of miR487b causes a complete shift in the targetome of the microRNA. The miR487b-ED-targetome is enriched for angiogenesis-associated pathways and functional assays demonstrated that miR487b-ED is pro-angiogenic whereas miR487b-WT is not. Moreover, we found that miR487b-ED's targetome is actively repressed during neovascularization after ischemia. Our findings suggest that editing of miR487b plays an intricate role in the regulation of post-ischemic neovascularization.



## ACKNOWLEDGEMENTS

We thank M. Eggenkamp and D. van den Homberg for their technical support.

*Sources of funding*

This study was supported by a grant from the Dutch Heart Foundation (Dr. E. Dekker Senior Postdoc, 2014T102).

*Disclosures*

None.

## REFERENCES


1. van Oostrom MC, van Oostrom O, Quax PH, Verhaar MC, Hoefer IE. Insights into mechanisms behind arteriogenesis: what does the future hold? *Journal of leukocyte biology*. 2008;84:1379-1391
2. Raval Z, Losordo DW. Cell Therapy of Peripheral Arterial Disease: From Experimental Findings to Clinical Trials. *Circ Res*. 2013;112:1288-1302
3. Welten SM, Bastiaansen AJ, de Jong RC, de Vries MR, Peters EA, Boonstra MC, Sheikh SP, La Monica N, Kandimalla ER, Quax PH, Nossent AY. Inhibition of 14q32 MicroRNAs miR-329, miR-487b, miR-494, and miR-495 increases neovascularization and blood flow recovery after ischemia. *Circ Res*. 2014;115:696-708
4. Welten SM, Goossens EA, Quax PH, Nossent AY. The multifactorial nature of microRNAs in vascular remodelling. *Cardiovasc Res*. 2016;110:6-22
5. Ha M, Kim VN. Regulation of microRNA biogenesis. *Nat Rev Mol Cell Biol*. 2014;15:509-524
6. Romaine SP, Tomaszewski M, Condorelli G, Samani NJ. MicroRNAs in cardiovascular disease: an introduction for clinicians. *Heart (British Cardiac Society)*. 2015;101:921-928
7. Nossent AY, Eskildsen TV, Andersen LB, Bie P, Bronnum H, Schneider M, Andersen DC, Welten SM, Jeppesen PL, Hamming JF, Hansen JL, Quax PH, Sheikh SP. The 14q32 microRNA-487b targets the antiapoptotic insulin receptor substrate 1 in hypertension-induced remodeling of the aorta. *Ann Surg*. 2013;258:743-751
8. Agarwal V, Bell GW, Nam JW, Bartel DP. Predicting effective microRNA target sites in mammalian mRNAs. *eLife*. 2015;4
9. Shafik A, Schumann U, Evers M, Sibbritt T, Preiss T. The emerging epitranscriptomics of long noncoding RNAs. *Biochimica et biophysica acta*. 2016;1859:59-70
10. Wulff B-E, Sakurai M, Nishikura K. Elucidating the inosinome: global approaches to adenosine-to-inosine RNA editing. *Nat Rev Genet*. 2010;12:81-85
11. Nishikura K. A-to-I editing of coding and non-coding RNAs by ADARs. *Nat Rev Mol Cell Biol*. 2016;17:83-96
12. Stellos K, Gatsiou A, Stamatelopoulos K, et al. Adenosine-to-inosine RNA editing controls cathepsin S expression in atherosclerosis by enabling HuR-mediated post-transcriptional regulation. *Nat Med*. 2016;22:1140-1150
13. Yi-Brunozzi HY, Easterwood LM, Kamilar GM, Beal PA. Synthetic substrate analogs for the RNA-editing adenosine deaminase ADAR-2. *Nucleic Acids Res*. 1999;27:2912-2917
14. Vitali P, Basyuk E, Le Meur E, Bertrand E, Muscatelli F, Cavaillé J, Huttenhofer A. ADAR2-mediated editing of RNA substrates in the nucleolus is inhibited by C/D small nucleolar RNAs. *J Cell Biol*. 2005:745-753.
15. Mizrahi RA, Phelps KJ, Ching AY, Beal PA. Nucleoside analog studies indicate mechanistic differences between RNA-editing adenosine deaminases. *Nucleic Acids Res*. 2012;40:9825-9835
16. Bachellerie JP, Cavaille J, Huttenhofer A. The expanding snoRNA world. *Biochimie*. 2002;84:775-790
17. Kawahara Y, Megraw M, Kreider E, Iizasa H, Valente L, Hatzigeorgiou AG, Nishikura K. Frequency and fate of microRNA editing in human brain. *Nucleic Acids Res*. 2008;36:5270-5280
18. Ekdahl Y, Farahani HS, Behm M, Lagergren J, Ohman M. A-to-I editing of microRNAs in the mammalian brain increases during development. *Genome Res*. 2012;22:1477-1487
19. Choudhury Y, Tay FC, Lam DH, Sandanaraj E, Tang C, Ang BT, Wang S. Attenuated adenosine-to-inosine editing of microRNA-376a* promotes invasiveness of glioblastoma cells. *The Journal of clinical investigation*. 2012;122:4059-4076

20. Kawahara Y, Zinshteyn B, Sethupathy P, Iizasa H, Hatzigeorgiou AG, Nishikura K. Redirection of silencing targets by adenosine-to-inosine editing of miRNAs. *Science*. 2007;315:1137-1140
21. Dong ZW, Shao P, Diao LT, Zhou H, Yu CH, Qu LH. RTL-P: a sensitive approach for detecting sites of 2'-O-methylation in RNA molecules. *Nucleic Acids Res*. 2012;40:e157-e157
22. Baker M, Robinson SD, Lechertier T, Barber PR, Tavora B, D'Amico G, Jones DT, Vojnovic B, Hodivala-Dilke K. Use of the mouse aortic ring assay to study angiogenesis. *Nat Protoc*. 2011;7:89-104
23. Ota H, Sakurai M, Gupta R, Valente L, Wulff BE, Ariyoshi K, Iizasa H, Davuluri RV, Nishikura K. ADAR1 forms a complex with Dicer to promote microRNA processing and RNA-induced gene silencing. *Cell*. 2013;153:575-589
24. Qi L, Song Y, Chan THM, et al. An RNA editing/dsRNA binding-independent gene regulatory mechanism of ADARs and its clinical implication in cancer. *Nucleic Acids Res*. 2017
25. Kanellos I, Vergoulis T, Sacharidis D, Dalamagas T, Hatzigeorgiou AG, Sartzetakis S, Sellis TK. MR-microT: a MapReduce-based MicroRNA target prediction method. *SSDBM 2014*. 2014:47:41-47:44
26. Paraskevopoulou MD, Georgakilas G, Kostoulas N, Vlachos IS, Vergoulis T, Reczko M, Filippidis C, Dalamagas T, Hatzigeorgiou AG. DIANA-microT web server v5.0: service integration into miRNA functional analysis workflows. *Nucleic Acids Res*. 2013;41:W169-173
27. van Rooij E, Olson EN. MicroRNA therapeutics for cardiovascular disease: opportunities and obstacles. *Nature reviews. Drug discovery*. 2012;11:860-872
28. Nossent AY, Bastiaansen AJ, Peters EA, de Vries MR, Aref Z, Welten SM, de Jager SC, van der Pouw Kraan TC, Quax PH. CCR7-CCL19/CCL21 Axis is Essential for Effective Arteriogenesis in a Murine Model of Hindlimb Ischemia. *Journal of the American Heart Association*. 2017;6
29. Nigita G, Acunzo M, Romano G, Veneziano D, Lagana A, Vitiello M, Wernicke D, Ferro A, Croce CM. microRNA editing in seed region aligns with cellular changes in hypoxic conditions. *Nucleic Acids Res*. 2016;44:6298-6308
30. Scholz D, Ziegelhoeffer T, Helisch A, Wagner S, Friedrich C, Podzuweit T, Schaper W. Contribution of arteriogenesis and angiogenesis to postocclusive hindlimb perfusion in mice. *Journal of molecular and cellular cardiology*. 2002;34:775-787
31. Hellingman AA, Bastiaansen AJ, de Vries MR, Seghers L, Lijkwan MA, Lowik CW, Hamming JF, Quax PH. Variations in surgical procedures for hind limb ischaemia mouse models result in differences in collateral formation. *European journal of vascular and endovascular surgery : the official journal of the European Society for Vascular Surgery*. 2010;40:796-803
32. Kiran AM, O'Mahony JJ, Sanjeev K, Baranov PV. Darned in 2013: inclusion of model organisms and linking with Wikipedia. *Nucleic Acids Res*. 2013;41:D258-261
33. Ramaswami G, Li JB. RADAR: a rigorously annotated database of A-to-I RNA editing. *Nucleic Acids Res*. 2014;42:D109-113
34. Picardi E, D'Erchia AM, Lo Giudice C, Pesole G. REDIportal: a comprehensive database of A-to-I RNA editing events in humans. *Nucleic Acids Res*. 2017;45:D750-757
35. Vitsios DM, Davis MP, van Dongen S, Enright AJ. Large-scale analysis of microRNA expression, epi-transcriptomic features and biogenesis. *Nucleic Acids Res*. 2016
36. Yang W, Chendrimada TP, Wang Q, Higuchi M, Seeburg PH, Shiekhattar R, Nishikura K. Modulation of microRNA processing and expression through RNA editing by ADAR deaminases. *Nat Struct Mol Biol*. 2006;13:13-21
37. Nishikura K. Functions and regulation of RNA editing by ADAR deaminases. *Annu Rev Biochem*. 2010;79:321-349

38. Bass BL. RNA editing by adenosine deaminases that act on RNA. *Annu Rev Biochem*. 2002;71:817-846
39. Lai F, Chen CX, Lee VM, Nishikura K. Dramatic increase of the RNA editing for glutamate receptor subunits during terminal differentiation of clonal human neurons. *J Neurochem*. 1997;69:43-52
40. Liu Y, Emeson RB, Samuel CE. Serotonin-2C receptor pre-mRNA editing in rat brain and in vitro by splice site variants of the interferon-inducible double-stranded RNA-specific adenosine deaminase ADAR1. *J Biol Chem*. 1999;274:18351-18358
41. Tripathi S, Flobak A, Chawla K, Baudot A, Bruland T, Thommesen L, Kuiper M, Laegreid A. The gastrin and cholecystokinin receptors mediated signaling network: a scaffold for data analysis and new hypotheses on regulatory mechanisms. *BMC systems biology*. 2015;9:40
42. Hermans KC, Blankesteijn WM. Wnt Signaling in Cardiac Disease. *Comprehensive Physiology*. 2015;5:1183-1209
43. Shoshan E, Mobley AK, Braeuer RR, et al. Reduced adenosine-to-inosine miR-455-5p editing promotes melanoma growth and metastasis. *Nat Cell Bio*. 2015;17:311-321

# CHAPTER 4

## Supplemental Materials

**Supplemental Tables**

I. Primer sequences and purpose
II. Sequences of sDNA and siRNAs
III. Enriched pathways of miR487b putative targetomes
Publications linking enriched pathways to neovascularization

**Supplemental Figures**

I. Characterization of the qPCR primer sets employed by serial dilution.
II. Reverse Transcription at Low deoxyribonucleoside triphosphate followed by Quantitative PCR (RTL-Q) of pri-miR487b.
III. Relative expression of miR487b-WT and miR487b-ED after HLI.
IV. Conservation of editing and expression of ADAR1, ADAR2 and Fibrillarin in primary human vascular cells.
V. miR487b-WT and miR487b-ED binding sites in the 3'UTR of IRS1.
VI. Six distinct miR487b-ED binding sites found in BMP1.
VII. Expression of unedited and edited putative targetomes in the adductor muscle.
VIII. MiR487b-WT and miR487b-ED overexpression in aortic rings and primary human fibroblasts and endothelial cells.
IX. Murine *Adar1*, *Adar2* and *Fibrillarin* mRNA expression in whole genome analysis of the adductor muscle before and after induction of HLI.

**Supplemental References**

## DETAILED METHODS

*Hindlimb Ischemia Model*

All animal experiments performed were approved by the committee on animal welfare of the Leiden University Medical Center (Leiden, The Netherlands. Approval reference number 09163).

Adult C57Bl/6 mice, 8 to 12 weeks old (Charles River) were housed in groups of 3 to 5 animals, with free access to tap water and regular chow. Only male mice were used since there is higher incidence of peripheral arterial disease, which this mouse model mimics, in men[1]. Furthermore, in our extensive experience with the hindlimb ischemia model, we also found that males and females respond differently, therefore we focus on the response in males for increased clinical relevancy.

For the induction of HLI, mice were anesthetized by intraperitoneal injection of midazolam (8 mg/kg, Roche Diagnostics), medetomidine (0.4 mg/kg, Orion) and fentanyl (0.08 mg/kg, Janssen Pharmaceuticals). Unilateral HLI was induced by electrocoagulation of the left femoral artery proximal to the superficial epigastric arteries. After surgery, anesthesia was antagonized with flumazenil (0.7 mg/kg, Fresenius Kabi), atipamezole (3.3 mg/kg, Orion) and buprenorphine (0.2 mg/kg, MSD Animal Health). Mice were sacrificed by cervical dislocation and the adductor and gastrocnemius muscles were excised en bloc and snap-frozen on dry ice before (T0) and at 1, 3 and 7 days (T1, T3 and T7 respectively) after induction of HLI. Muscle tissues were crushed with mortar and pestle, while using liquid nitrogen to preserve sample integrity, and were stored at -80°C afterwards until continuation of experiments.

The assignment of the mice to the experimental groups was conducted randomly. All animals were included in the study and the definition of inclusion and exclusion criteria as well as primary and secondary endpoints was not applicable. Due to exploratory nature of the research (vide supra) a power and sample size calculations were not possible. Aortic ring assays were analysed by a blinded investigator.

*RNA isolation and cDNA synthesis*

Total RNA was isolated according to standard protocol using TRIzol Reagent (Life Technologies) after which sample concentration and purity were examined by nanodrop (Nanodrop Technologies). DNase treatment using RQ1 RNase-Free DNase

(Promega) was performed according to manufacturer's instructions. Complementary DNA (cDNA) was prepared using the High Capacity cDNA Reverse Transcription Kit (Applied Biosystems) according to manufacturer's protocol.

*Pri-miR487b Sanger sequencing*

Genomic DNA (gDNA) was isolated from murine tissue using DNeasy Blood & Tissue Kits (Qiagen) to serve as reference. PCR was performed to amplify the pri-miR487b sequence from 3 different DNA samples and 12 different murine muscle tissue cDNA samples with GoTaq DNA Polymerase (Promega) (for primer sequences, see **Supplemental Table I**). Gel electrophoresis of the product was performed after which the correctly sized DNA band was excised and purified using Wizard SV Gel and PCR Clean-Up System (Promega).



Amplified and purified gDNA and cDNA samples were prepared and submitted for Sanger sequencing to the Leiden Genome Technology Center (Leiden, the Netherlands) according to their instructions.

On return, chromatograms of cDNA samples were compared to chromatograms of mouse gDNA. Since A-to-I-editing presents itself as A-to-G substitutions on chromatograms, the location of each gDNA adenosine was analyzed for presence of a secondary guanosine peak in the cDNA samples. Only consistent observations of a secondary guanosine peak at the genomic location of an adenosine across samples were considered to be A-to-I-editing.

*Selective digestion of pri-miR487b-WT but not pri-miR487b-ED*

Two synthetic oligonucleotides were purchased from Sigma-Aldrich as positive and negative controls: one with the sequence of unedited (A) pri-miR487b and one with that of edited (G) pri-miR487b (sequences, see **Supplemental Table II**). The synthetic oligonucleotides were amplified using pri-miR487b primers (for primer sequences, see **Supplemental Table I**). The pri-miR487b sequence was amplified from cDNA. PCR products were purified as described above. Amplification products were digested with FastDigest PfeI* (Thermo Scientific) for 90 minutes at 37°C to ensure complete digestion of all samples. Cleavage products were separated by gel electrophoresis. Objective densitometric quantification of the bands was performed using ImageJ software. To ensure fluctuations in amount of pri-miR487b-WT are also

accounted for, A-to-I-editing was expressed as the intensity of the uncut band (G) as a percentage of combined intensity of both cut (A) and uncut (G) bands.

*MicroRNA rt/qPCR*

Quantification of mature unedited miR487b (miR487b-WT) was performed according to manufacturer's protocol using a TaqMan miR assay (Applied Biosystems). For quantification of mature edited miR487b (miR487b-ED), a custom TaqMan Small RNA Assay (Applied Biosystems) specifically targeting the sequence 'A**G**UCGUACAGGGUCAUCCACU' was used. Samples for qPCR were run in triplicate on a ViiA 7 Real-Time PCR System (Applied Biosystems). Efficiency of both rt/qPCR kits was characterized using serial dilution (**Supplemental Figure I A**). Percentage miR487b-ED was calculated by measuring both miR487b-ED and miR487b-WT and expressing miR487b-ED as a percentage of the combined expression of both miR487b-WT and –ED. Relative expression of miR487b-ED and miR487b-WT was calculated using a reference microRNA that was predetermined to be stable across all sample types and experimental conditions of a particular experiment. For relative microRNA expression in murine tissue samples, Let-7c was used as reference, since its expression was stable across murine tissue types and before and after induction of ischemia. In human primary cell cultures, miR-191 was used as reference instead, because it was stably expressed across investigated human cell types whereas Let-7c was not.

*Isolation of human umbilical arterial fibroblasts and smooth muscle cells (HUAFs & HUASMCs) and human umbilical venous endothelial cells (HUVECs)*

Isolation and culturing of primary arterial human umbilical cells was performed as described by Welten *et al*[2]. In brief, umbilical cords were collected from full-term pregnancies and stored in sterile PBS at 4°C and subsequently used for cell isolation within 5 days. The arteries were removed and cleaned and tunica adventitia and tunica media were separated after removal of arterial endothelial calls by gently rolling the artery over a blunted needle. After overnight incubation in HUASMC culture medium (DMEM GlutaMAX™ (Invitrogen, GIBCO, Auckland, New Zealand), 10% heat inactivated fetal bovine serum (PAA), 10% heat inactivated human serum, 1% penicillin/streptomycin and 1% nonessential amino acids (PAA)) both tunicae were incubated in a 2mg/ml collagenase type II solution (Worthington) at 37 °C. The cell

suspension was filtered over a 70µm cell strainer and centrifuged at 400g for 10 minutes. The cell pellets were resuspended and plated in culture medium (HUAF culture medium: DMEM GlutaMAX™ (Invitrogen, GIBCO, Auckland, New Zealand), 10% heat inactivated fetal bovine serum (PAA) and 1% penicillin/streptomycin (MP Biomedicals, Solon, OH, USA)). Cells isolated from the tunica adventitia were washed with culture medium after 90 minutes to remove slow-adhering non-fibroblast cells.

For HUVEC isolation, cannulas were inserted on each side of the vein of an umbilical cord and flushed with sterile PBS. The artery was infused with 0.075% collagenase type II (Worthington, Lakewood, NJ, USA) and incubated at 37°C for 20 minutes. The collagenase solution was collected and the artery was flushed with PBS in order to collect all detached endothelial cells. The cell suspension was centrifuged at 400 g for 5 minutes and the pellet was resuspended in HUVEC culture medium (M199 (PAA, Pasching, Austria), 10% heat inactivated human serum (PAA), 10% heat inactivated newborn calf serum (PAA), 1% penicillin/streptomycin, 150µg/ml endothelial cell growth factor (kindly provided by Dr. Koolwijk, VU Medical Center, Amsterdam, the Netherlands) and 0.1% heparin (LEO Pharma, Ballerup Danmark)). HUVECs were cultured in plates coated with 1% fibronectin.



*Primary cell culture*

Cells were cultured at 37°C in a humidified 5% $CO_2$ environment. Culture medium was refreshed every 2-3 days. Cells were passed using trypsin-EDTA (Sigma, Steinheim, Germany) at 90-100% (HUASMCs and HUVECs) or 70-80% confluency (HUAFs). HUAFs were used up to passage five and HUASMCs and HUVECs up to passage three. Stock solutions of isolated HUASMCs, HUAFs and HUVECs up to passage two were stored at -18 °C in DMEM GlutaMAX™ containing 20% FBS and 10% DMSO (Sigma).

*RNA binding protein immunoprecipitation*

RNA binding protein immunoprecipitation (RIP) was performed using the EZMagna RIP kit (Millipore). HUAF cells were grown to 90% confluency, trypsinized and pelleted at 300g using a table-top centrifuge. Cell pellet was resuspended in 0.4% formaldehyde for crosslinking of RNA-protein complexes. Next, cells were pelleted again and resuspended in complete RIP lysis buffer. Cell lysates were incubated with RIP buffer containing magnetic beads conjugated with antibodies against ADAR1

(Abcam ab168809), ADAR2 (Abcam ab64830), Fibrillarin (Abcam ab5821) and negative control rabbit control IgG (Millipore PP64B). Before immunoprecipitation, 10% of cell lysate was taken to serve as input reference. Next, samples were treated with proteinase K to digest protein and RNA was isolated and cDNA was made as described above. qPCRs for the precursor miR487b transcript were run in triplicate on the cDNA of each IP fraction using QuantiTect SYBR Green PCR Kit (Qiagen) to determine if binding of this transcript to the immunoprecipitated proteins is enriched compared to immunoprecipitation of the negative control (for primer sequences, see **Supplemental Table I**).

*RTL-Q*

To confirm and quantify 2'OMe of miR487b, we performed Reverse Transcription at Low deoxyribonucleoside triphosphate followed by Quantitative PCR (RTL-Q), a modification to the RTL-P method, described by Dong *et al*[3] (**Supplemental Figure II**). This method relies on the fact that 2'OMe of RNA hinders primer extension during reverse transcription when the reaction is performed at very low dNTP concentrations.

In short, four different RT primers were designed around the site of interest (**Supplemental Table I**) and used for individual reverse transcription reactions at low dNTPs (0.5uM) and high dNTPs (200uM) as described by Dong *et al*[25]. Afterward we performed qPCR using SYBR green as above to quantify differences in primer extension, followed by estimation methylated fraction according to Aschenbrenner and Marx's methodology[4], instead of using endpoint PCR. Both murine and human RTL-Q-qPCR primer sets were characterized in order to include amplification efficiencies into the calculations (**Supplemental Figure I B**).

*In silico target prediction and pathway enrichment analysis*

Diana-MR-microT software (diana.imis.athena-innovation.gr) was employed to predict the group of genes targeted by miR487b-WT and miR487b-ED, constituting their individual targetome. This software allows for custom microRNA-sequence prediction[5]. MiR487b-WT's targetome was predicted by submitting its sequence (A**A**UCGUACAGGGUCAUCCACU) and 'A**G**UCGUACAGGGUCAUCCACU' was submitted for miR487b-ED's putative targetome. No restrictions were applied for target prediction, but in addition to target gene name, microRNA binding location and

microRNA binding type, Diana binding score was recorded. Binding score is based on predicted binding thermodynamics, where binding score closer to 1 indicates a stronger predictive interaction between microRNA and target gene.

Changes in targeted gene pathways after miR487b editing were analysed using PANTHER pathway enrichment analysis (www.pantherdb.org) on the resulting lists of target genes as described previously[6].

*Dual Luciferase Reporter Gene Assays*

Constructs: A fragment of 519 bp of the *IRS1* 3'UTR and for *BMP1* two separate fragments of 833 bp and 596 bp were amplified from human cDNA using primers with a short extension, containing cleavage sites for XhoI (5'-end) and NotI (3'-end) (**Supplemental Table I**). Amplicons were digested with XhoI and NotI and cloned in between the XhoI and NotI cleavage sites of the PsiCHECK™-2 vector (Promega) at the 3'-end of the coding region of the Renilla luciferase reporter gene. The cloned sequence was confirmed using Sanger sequencing. The Phusion Site-Directed Mutagenesis Kit (Thermo Scientific) was used to create multiple vectors with predicted binding sites for both miR487b-WT and miR487b-ED, as summarized in **Figure 5B&C**. Successful mutagenesis was confirmed using Sanger sequencing. Sequences of the primers used are available in **Supplemental Table I**.

Luciferase Assays: HeLa cells were cultured at 37°C under 5% $CO_2$ using DMEM (Gibco) with high glucose and stable L-glutamine, supplemented with 10% fetal calf serum and Penicillin/Streptomycin. For experiments, HeLa cells were grown to 75-80% confluence in white 96 well plates in their normal growth medium, at 37°C under 5% $CO_2$. Lipofectamine 2000 (Invitrogen) in Opti-MEM (Gibco) was used according to manufacturer's instructions to transfect the cells with 20 ng of either the PsiCHECK2-vector containing endogenous or mutant miR487b binding sequences behind the coding sequence for Renilla Luciferase or the original empty vector. Cells were co-transfected with pre-miR487b-WT, pre-miR487b-ED, negative control pre-miR (Ambion, Applied Biosystems) or vehicle at a concentration of 10 nM. Firefly- and Renilla-luciferase were measured in cell lysates using a Dual-Luciferase Reporter Assay System (Promega) according to manufacturer's protocol on a Cytation™ 5 plate reader (BioTek). Firefly luciferase activity was used as an internal control for cellular density

and transfection efficiency. The luminescence ratios were corrected for differences in baseline vector luminescence observed in vehicle treated group and expressed as fraction of scrambled control luminescence.

Displayed luciferase data were obtained from at least three independent experiments.

*In vivo miR487b Putative Targetome Expression*

To assess the impact of miR487b editing on targetome expression, we used a previously published whole genome expression microarray dataset (Nossent *et al*[7]). For each gene detected above background levels (21074 out of 45200), post-ischemic expression was calculated relative to its expression before HLI by calculating the $2^{\Delta \text{Log}2(\text{measured gene intensity})}$. Average putative targetome expression was then calculated by averaging the fold expression of all genes within the particular targetome. Targetome expressions were compared expression of the average expression of all genes above detection limit.

*siRNA knockdown of ADAR1, ADAR2 and Fibrillarin*

HUAFs were seeded in 12 wells plates and grown overnight. At 70% confluence the cells were transfected using Lipofectamine RNAiMax (Invitrogen), according to the manufacturer's protocol, with a final concentration of 27.5 nM siRNA. For control siRNA and the siRNAs knocking down ADAR1 and ADAR2 the following previously validated siRNA sequences were used[8]:

siADAR1: 5′-GCUAUUUGCUGUCGUGUCA(dT)(dT)-3′;

siADAR2: 5′-GAUCGUGGCCUUGCAUUAA(dT)(dT)-3′;

Scrambled: 5′-UCUCUCACAACGGGCAU(dT)(dT)-3′

The siRNA used to knockdown *Fibrillarin* was SASI_Hs01_00095018, a MISSION® Predesigned siRNA purchased from Sigma-Aldrich.

After 48 hours, cells were washed 3 times with PBS and total RNA was isolated and cDNA was synthesized as before. Expression of *ADAR1*, *ADAR2*, *Fibrillarin* and *RPLP0* (used as stable housekeeping gene) was measured using SYBR Green qPCR as above, with intron spanning primers (for primer sequences, see **Supplemental Table I**). Subsequent miR487b expression, editing and methylation analyses were performed as described before.

*Transfection of miR487b-WT or miR487b-ED for target validation and scratch assay*

The effects of miR487b-WT or miR487b-ED overexpression on scratch-wound healing of HUAFs and HUVECs were also examined since coordinated cell migration is an essential factor in neovascularization[9,10]. For scratch assays HUAFs and HUVECs were seeded in 12 wells plates and grown overnight. At 80% confluence medium was replaced with low serum culture medium (HUAFs: 0.1% instead of 10% FCS; HUVECS: just 10% FCS instead of 10% FCS and 10% HS) to which pre-miR487b-WT, pre-miR487b-ED or negative control pre-miRNA were added at a final concentration of 1nM. After 24h, medium was removed and a scratch-wound was introduced across the diameter of each well of a 12 wells plate using a p200 pipette tip. Subsequently, the cells were washed with PBS and medium was replaced by new low serum culture medium containing the same pre-miRNA. Two locations along the scratch-wound were marked per well and scratch-wound closure at these sites was imaged by taking pictures at time 0h and 18h after scratch-wound introduction using live phase-contrast microscopy (Axiovert 40C, Carl Zeiss). After pictures at 18h were taken, cells were washed 3 times in PBS and then lysed and harvested in TRIzol for RNA isolation and miR487b expression was determined as before. Average scratch-wound closure after 18h was objectively calculated per well by measuring difference in cell coverage at 18h vs 0h using the wound healing tool macro for ImageJ.

For target *in vitro* target validation studies, HUAFs and HUVECs were seeded and cultured similar to for scratch assays, however, 100nM pre-miRNA concentrations were used instead. The pre-miRNA containing low serum culture medium was also refreshed after 24h, and after 18h more hours of incubation these, these cells were also harvested similarly. However, after RNA isolation, total cDNA synthesis was performed instead and target gene expression was measured using SYBR Green qPCR as above employing intron spanning primers and RPLP0 as stable reference gene RPLP0 (for primer sequences, see **Supplemental Table I**).

*Aortic Ring Assay*

Mouse aortic ring assays were performed as described previously[2,11]. In brief, six thoracic aortas were removed from 8 to 10-week old mice, after which the surrounding fat and branching vessels were carefully removed and the aorta was flushed with Opti-

MEM (Gibco). Aortic rings of ~1 mm were cut and the rings from each mouse aorta were divided into four groups and incubated overnight with fresh Opti-MEM containing either pre-miR487b-WT, pre-miR487b-ED or negative control pre-miR with a final concentration of 100nM.

96-well plates were coated with 75 µl collagen matrix (Collagen (Type I, Millipore) diluted in 1x DMEM (Gibco) and pH adjusted with 5N NaOH). One aortic ring per well was embedded in the collagen matrix, for a total of 15 rings per pre-miRNA treatment. After letting the collagen solidify for an hour, 150 µl Opti-MEM supplemented with 2.5% FBS (PAA, Austria), penicillin-streptomycin (PAA, Austria) and 30ng/ml VEGF (R&D systems) and pre-miRNAs was added to each well. Medium was refreshed first on day 3, then every other day. Pictures of each embedded aortic ring and their neovessel outgrowth were made after 7 days using live phase-contrast microscopy (Axiovert 40C, Carl Zeiss). The number of neovessel sprouts were counted manually. Each neovessel emerging from the ring was counted as a sprout and individual branches arising from each microvessel counted as a separate sprout.

For immunohistochemistry the embedded rings were formalin fixed and permeabilized with 0.25% Triton X-100. A triple staining was performed using primary antibodies against smooth muscle cells (α-smooth muscle actin, 1A4, DAKO), endothelial cells (CD31, BD Pharmingen) and fibroblasts (Vimentin Abcam). Alexa Fluor 647, Alexa Fluor 488 and Alexa Fluor 594 antibodies (Life Technologies) were used as secondary antibodies and slides were mounted with Fluoroshield with DAPI (Sigma-Aldrich). Images were captured with a LSM700 confocal laser-scanning microscope (Zeiss).

For quantification of miR487b overexpression in aortic rings the rings that remained after embedding 15 per treatment group were used. These aortic rings were incubated alongside the embedded rings in a single 24-wells-plate-well per treatment, receiving similar medium changes containing the same amount of pre-miRNAs. After 7 days of pre-miRNA incubation, these rings were washed 3 times with PBS , snap frozen with liquid nitrogen and homogenized for subsequent RNA isolation using TRIzol. Finally, miR487b quantification was done as described previously.

*Statistical Analysis*

All results are expressed as mean ± SEM. Normality of data obtained was examined using the Shapiro-Wilk normality test. Since all variables measured were continuous parameters, pairwise comparisons were tested using unpaired, 2-tailed Student's *t*-tests. *P* values less than 0.05 were considered statistically significant.

# SUPPLEMENTAL TABLES

**Supplemental Table I:** Primer sequences and purpose

| Name | Primer type | Template | Experiment | Purpose | Sequence |
|---|---|---|---|---|---|
| MMU-pri-miR487b F | Forward | Murine c- and gDNA | Editing discovery and verification | Amp and Seq of cDNA and gDNA | CGGTGGCTTTGCTTTCCA |
| MMU-pri-miR487b R | Reverse | | | | CAGAGTCTGCGCACTTGA |
| HSA-pri-miR487b F | Forward | Human cDNA | Editing verification and to quantify pri-miRNA | Amp and qPCR of human cDNA | AGGCAGTGGCTTTCTTTTCC |
| HSA-pri-miR487b R | Reverse | | | | GAGGTGGGATCCAAACACAG |
| sDNA-pri-miR487b F | Forward | sDNA | Editing verification | Amp of sDNA | GCTTTGGTACTTGGAGAGTGG |
| sDNA-pri-miR487b R | Reverse | | | | TGCGCACTTGATACTGAAAAA |
| HSA-FBL-miR487b F | Forward | Human cDNA | Pri-miR487b association with FBL | qPCR of Fibrillarin-IP cDNA | CCTGTCCTGTTCGTTTTGCT |
| HSA-FBL-miR487b R | Reverse | | | | AAAGTGGATGACCCTGTACGA |
| pri-miR487b RT primer 1 | complementary | MMU and HSA cDNA | RTL-Q | Control primers for RT step | AAAAGTGGATGACCCTGTACG |
| pri-miR487b RT primer 2 | complementary | | | | AAAGTGGATGACCCTGTACGA |
| pri-miR487b RT primer 3 | complementary | MMU and HSA cDNA | RTL-Q | Experimental primer for RT step | AAGTGGATGACCCTGTACGAT |
| pri-miR487b RT primer 4 | complementary | | | | AGTGGATGACCCTGTACGATT |
| MMU-pri-miR487b RTL-Q F | forward | Murine cDNA | RTL-Q | qPCR primer | GAGAGTGGTTATCCCTGTCCTC |
| HSA-pri-miR487b RTL-Q F | forward | | | | CCTGTCCTGTTCGTTTTGCT |
| pri-miR487b RTL-Q R | reverse | MMU and HSA cDNA | | | GTGGATGACCCTGTACGATTC |
| HSA-IRS1 F | forward | Human cDNA | Luciferase assay | Amp and elongation of IRS1 3'UTR | ATACTCGAGTGACCTCAGCAAATCCTCTTC |
| HSA-IRS1 R | reverse | | | | ATAGCGGCCGCATACCTCCATCCCACATCCA |
| IRS1mutagenesis-site1 F | forward | WT IRS1 3'UTR Psicheck 2 vector | Luciferase assay | Mutate T to C: binding site from WT to ED | [Phos]AGATGGTACGA**C**GCATCCATTTCA |
| IRS1mutagenesis-site1 R | reverse | | | | [Phos]ACTGATGAGGAAGATATGAGGTCCTAGTTG |
| IRS1mutagenesis-site2 F | forward | WT IRS1 3'UTR Psicheck 2 vector | Luciferase assay | Mutate C to T: binding site from ED to WT | [Phos]AACTGTGTACGA**T**AAAGCATCATTG |
| IRS1mutagenesis-site2 R | reverse | | | | [Phos]TCAGCAGCAGATGAAATGTATC |
| HSA-BMP1 F1 | forward | Human cDNA | Luciferase assay | Amp and elongation of BMP1 part1 | ATACTCGAGACGTCCCTGGACCTGTACC |
| HSA-BMP1 R1 | reverse | | | | ATAGCGGCCGCCAGCTTGGAGTCAGCTGTGA |

| | | | | | |
|---|---|---|---|---|---|
| HSA-BMP1 F2 | forward | Human cDNA | Luciferase assay | Amp and elongation of BMP1 part2 | ATACTCGAGCAACACGTTCGGCAGTTATG |
| HSA-BMP1 R2 | reverse | | | | ATAGCGGCCGCAGGCCCTGAGCCACAGTAG |
| BMP1mutagenesis-site1 F | forward | BMP1 part 1 Psicheck 2 vector | Luciferase assay | Mutate C to T: binding site from ED to WT | [Phos]GTGCTGGTACGA**T**TATGTGGAGGTC |
| BMP1mutagenesis-site1 R | reverse | | | | [Phos]AGGCGGCTGCGGTACAGGT |
| BMP1mutagenesis-site2 F | forward | BMP1 part 1 Psicheck 2 vector | Luciferase assay | Mutate C to T: binding site from ED to WT | [Phos]CTGTGCCTACGA**T**TATCTGGAGGTG |
| BMP1mutagenesis-site2 R | reverse | | | | [Phos]CTGTCGTGGCGCTCAATCTC |
| BMP1mutagenesis-site3 F | forward | BMP1 part 1 Psicheck 2 vector | Luciferase assay | Mutate C to T: binding site from ED to WT | [Phos]GCAAGTACGA**T**TTCGTGGAGGT |
| BMP1mutagenesis-site3 R | reverse | | | | [Phos]ACACATCATTGCCCTCTGTCTC |
| BMP1mutagenesis-site4 F | forward | BMP1 part 2 Psicheck 2 vector | Luciferase assay | Mutate C to T: binding site from ED to WT | [Phos]AACAAGCACGA**T**TGCAAAGAAGC |
| BMP1mutagenesis-site4 R | reverse | | | | [Phos]GTCATGGAGGACGAAGCCACT |
| BMP1mutagenesis-site5 F | forward | BMP1 part 2 Psicheck 2 vector | Luciferase assay | Mutate C to T: binding site from ED to WT | [Phos]GTGTGCCTACGA**T**CACCTAGAGG |
| BMP1mutagenesis-site5 R | reverse | | | | [Phos]TCAGGCTGGGACTCGATGT |
| BMP1mutagenesis-site6 F | forward | BMP1 part 2 Psicheck 2 vector | Luciferase assay | Mutate C to T: binding site from ED to WT | [Phos]CGACGGCTACGA**T**AGCACAGC |
| BMP1mutagenesis-site6 R | reverse | | | | [Phos]AAGAGCTCCATGTAGTCATAGCCGC |
| HSA-ADAR1 F | Forward | Human cDNA | Expression in primary cells | Measure expression | GCTTGGGAACAGGGAATCGC |
| HSA-ADAR1 R | Reverse | | | | CGCAGTCTGGGAGTTGTATTTC |
| HSA-ADAR2 F | Forward | Human cDNA | Expression in primary cells | Measure expression | GGAAGCTGCCTTGGGATCAG |
| HSA-ADAR2 R | Reverse | | | | GCTGCTGGAACTCATGTTTTCTTC |
| HSA-FBL F | Forward | Human cDNA | Expression in primary cells | Measure expression | CAGACCAGACCCGGATTGTG |
| HSA-FBL R | Reverse | | | | AGGCTGTGGAGTCAATGCAG |
| HSA-RPLP0 F | Forward | Human cDNA | Expression in primary cells | Reference household gene for mRNA expression | TCCTCGTGGAAGTGACATCG |
| HSA-RPLP0 R | Reverse | | | | TGTCTGCTCCCACAATGAAAC |
| HSA-GAPDH F | Forward | Human cDNA | Expression in primary cells | Reference household gene for mRNA expression | CACCACCATGGAGAAGGC |
| HSA-GAPDH R | Reverse | | | | AGCAGTTGGTGGTGCAGGA |
| HSA-U6 F | Forward | Human cDNA | Expression in primary cells | Reference household gene for pri-miRNA expression | AGAAGATTAGCATGGCCCCT |
| HSA-U6 R | Reverse | | | | ATTTGCGTGTCATCCTTGCG |

**Supplemental Table II:** Sequences of sDNA and siRNAs

| **Name and sequences of synthetic DNAs and short interfering RNAs** | |
|---|---|
| sDNA-pri-miR487b-WT:<br>GCTTTGGTACTTGGAGAGTGGTTATCCCTGTCCTCTTCGCTTCACTCATGCCG**AATCGTACAGGGTCATCCAC**TTTTTCAGT ATCAAGTGCGCA | |
| sDNA-pri-miR487b-ED:<br>GCTTTGGTACTTGGAGAGTGGTTATCCCTGTCCTCTTCGCTTCACTCATGCCG**AGTCGTACAGGGTCATCCAC**TTTTTCAGT ATCAAGTGCGCA | |
| siADAR1: | 5'-GCUAUUUGCUGUCGUGUCA(dT)(dT)-3' |
| siADAR2: | 5'-GAUCGUGGCCUUGCAUUAA(dT)(dT)-3' |
| siRNA control: | 5'-UCUCUCACAACGGGCAU(dT)(dT)-3' |
| siRNA FBL: | SASI_Hs01_00095018 (MISSION® Predesigned siRNA, Sigma-Aldrich) |

**Supplemental Table IIIa.** Enriched pathways of miR487b putative targetomes*

| | Total genes mapped to pathway | # of mapped genes in target set | Expected # of genes targeted | Fold Enrichment | *P* value |
|---|---|---|---|---|---|
| **miR487b-WT** | | | | | |
| Murine | 2607 | 258 | | | |
| CCKR signalling | 165 | 33 | 14.7 | 2.24 | 0.004 |
| Ras Pathway | 73 | 18 | 6.5 | 2.77 | 0.023 |
| PDGF signalling pathway | 140 | 27 | 12.5 | 2.16 | 0.036 |
| Insulin/IGF pathway | 34 | 11 | 3.0 | 3.63 | 0.049 |
| Human | 2639 | 250 | | | |
| - | | | | | |
| **miR487b-ED** | | | | | |
| Murine | 2607 | 346 | | | |
| Wnt signalling pathway | 304 | 65 | 29.8 | 2.18 | 0.000001 |
| Cadherin signalling pathway | 154 | 41 | 15.1 | 2.72 | 0.000004 |
| Human | 2639 | 269 | | | |
| Wnt signalling pathway | 311 | 52 | 27.9 | 1.86 | 0.004 |
| PDGF signalling pathway | 149 | 31 | 13.4 | 2.32 | 0.004 |
| Angiogenesis | 176 | 33 | 15.8 | 2.09 | 0.015 |
| Insulin/IGF pathway | 33 | 11 | 3 | 3.72 | 0.041 |

* Putative miR487b targetomes were analysed by the PANTHER pathway algorithm. Only pathway enrichments with *P*>0.05 after Bonferroni correction are reported.

**Supplemental Table IIIb:** Publications linking enriched pathways to neovascularization

| Signalling pathway | microRNA with targetome enrichment for pathway* | Publications linking pathway to*: | | | |
|---|---|---|---|---|---|
| | | Angio-genesis | Arterio-genesis | Ischemia | Vascular disease |
| CCKR signalling | MMU-miR487b-**WT** | 1 | 0 | 0 | 0 |
| Ras Pathway | MMU-miR487b-**WT** | 947 | 6 | 255 | 99 |
| PDGF signalling pathway | MMU-miR487b-**WT** HSA-miR487b-**ED** | 1063 | 26 | 166 | 96 |
| Insulin/IGF pathway | MMU-miR487b-**WT** HSA-miR487b-**ED** | 1630 | 7 | 1949 | 1446 |
| WNT signalling pathway | MMU-miR487b-**ED** HSA-miR487b-**ED** | 549 | 4 | 115 | 21 |
| Cadherin signalling pathway | MMU-miR487b-**ED** | 993 | 10 | 175 | 23 |
| Angiogenesis | MMU-miR487b-**ED** | 76634 | 500 | 3509 | 508 |

* Number of publications found when searching title and abstracts for the pathway name in combination with the indicated neovascularization associated terms in the PubMed database. MMU – Mus musculus; HSA - Homo sapiens

## SUPPLEMENTAL FIGURES

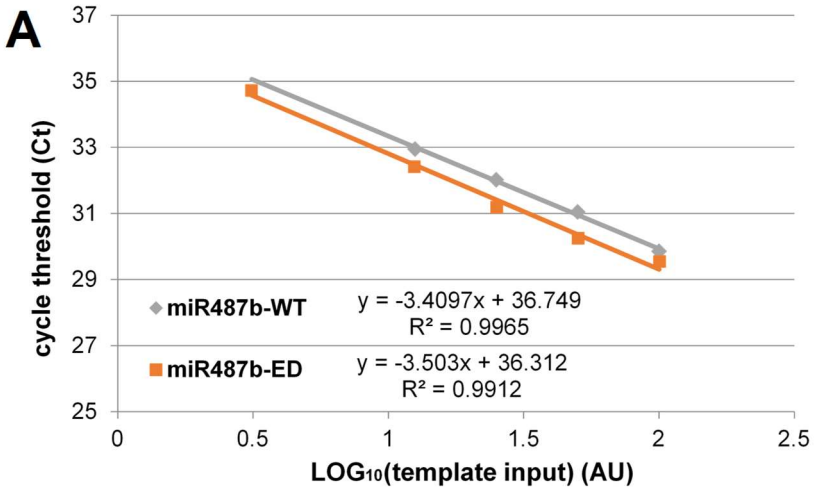


| | miR487b-WT | miR487b-ED |
|---|---|---|
| Slope | -3,4097 | -3,503 |
| Efficiency | 1,964631 | 1,92961 |

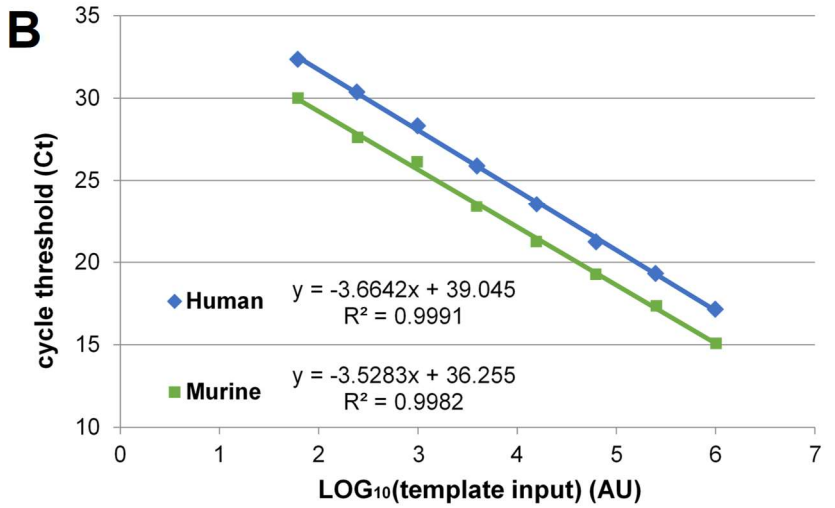


| | Human | Murine |
|---|---|---|
| Slope | -3,6642 | -3,5283 |
| Efficiency | 1,87461 | 1,920537 |

**Supplemental Figure I: Characterization of the qPCR primer sets employed by serial dilution.** (**A**) Characterization of qPCR efficiency (E) of TaqMan miR487b-WT and custom miR487b-ED rt/qPCR kits by serial dilution of human and murine cDNA measured in triplicate. (**B**) Characterization of qPCR efficiency the primer sets used in RTL-Q to quantify human and murine pri-miR487b by serial dilution of synthetic DNA measured in triplicate. In both cases, cycle threshold versus the log base 10 of relative input were plotted to calculate the slope. The equation $E = 10^{(-1/slope)}$ was used to calculate the corresponding real-time PCR efficiencies[12].

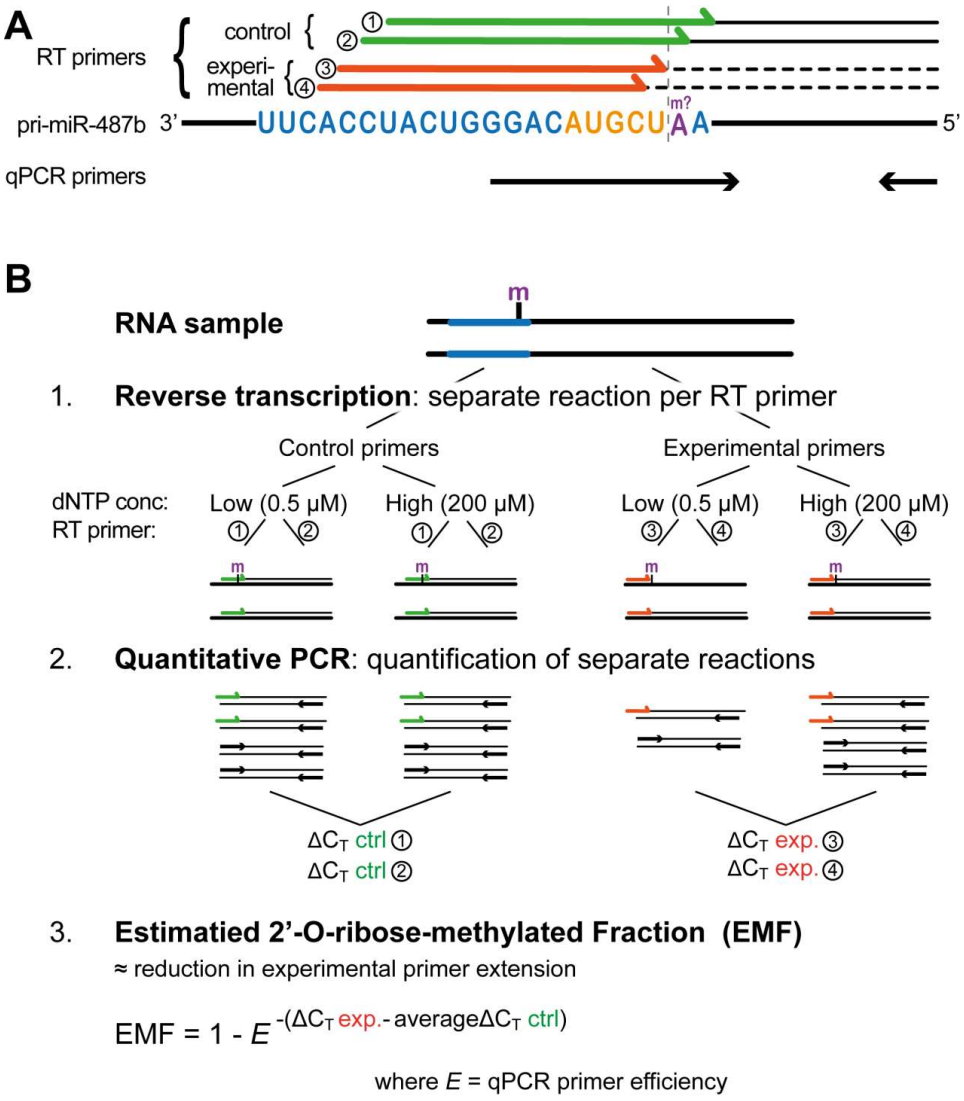


**Supplemental Figure II: Reverse Transcription at Low deoxyribonucleoside triphosphate followed by Quantitative PCR (RTL-Q) of pri-miR487b.** RTL-Q is a modified 2'-O-ribose-Methylation (2'OMe) detection method that allows for quantitative estimation of specific nucleotide 2'OMe. This method relies on the fact that 2'OMe of RNA hinders primer extension during reverse transcription when the reaction is performed at very low dNTP concentrations. As described by Dong *et al*[3], (**A**) four different RT primers were designed around the site of interest. Two of these primers cover the hypothetical pri-miR487b methylation site (in purple) and serve as control group. The other two primers end right before the site to be investigated, and thus extension of these experimental primers would be inhibited if 2'OMe is present specifically on pri-miR487b's 2+ adenosine. (**B**) To quantify this inhibition, the first step is to perform a total of eight reverse transcription reactions per sample, with individual reactions per RT primer at low dNTPs (0.5uM) and high dNTPs (200uM). Unlike Dong *et al*, we then performed qPCR to quantify the amount of primer extension in each sample. Next we calculated the difference in observed cycle threshold ($C_T$) between low and high dNTP reactions per RT primer, thereby employing the high dNTP reactions to serve as uninhibited reference for normalization. Finally, we used the formula described by Aschenbrenner and Marx[4] to quantify the Estimated 2'-O-ribose-methylated Fraction (EMF) per experimental RT primer. This calculation is based on the conservative assumption that 2'OMe inhibits all primer extension, therefore equating EMF to the relative reduction in experimental primer extension after adjusting for the qPCRs amplification efficiency.

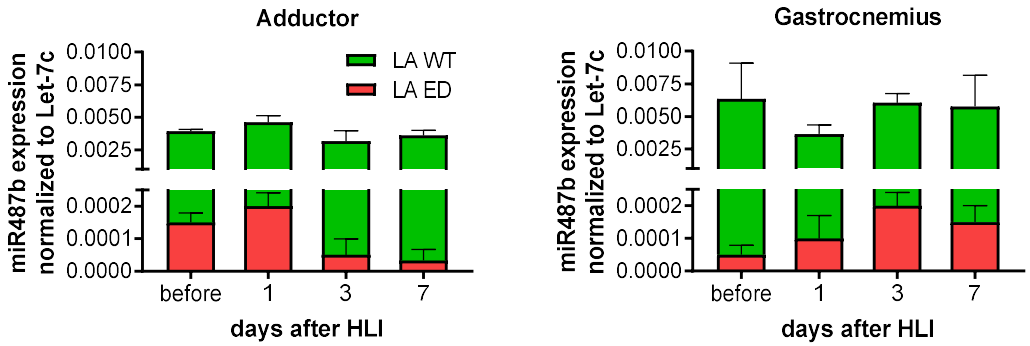


**Supplemental Figure III: Relative expression of miR487b-WT and miR487b-ED after HLI.** Relative expression of mature miR487b-WT (green) and miR487b-ED (red) in cDNA from adductor and gastrocnemius muscle before and after hindlimb ischemia (HLI) quantified by rt/qPCR. Data is presented as mean ± SEM (3 or 4 mice per timepoint) and corresponds with that of **Figure 2D**. This time, data is normalized to stable reference miRNA Let-7c instead to reflect absolute changes in miR487b-ED expression after HLI.

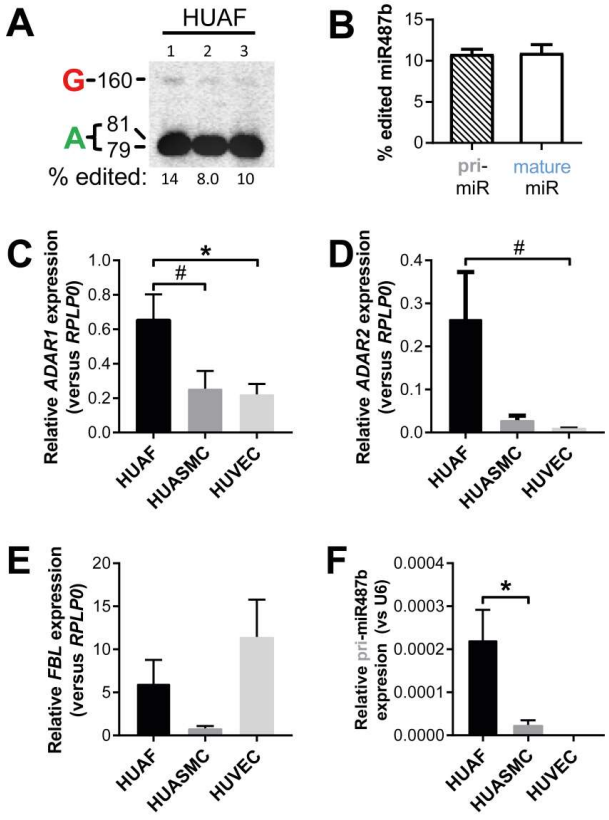


**Supplemental Figure IV: Conservation of editing and expression of *ADAR1*, *ADAR2* and *Fibrillarin* in primary human vascular cells.** (**A**) PfeI digestion of amplified pri-miR487b from human umbilical arterial fibroblast (HUAF) cDNA. (**B**) Quantification of percent edited pri-miR487b displayed in (**E**) and mature miR487b in HUAFs (n=3) by rt/qPCR. (**C-F**) Expression of *ADAR1*, *ADAR2* and *Fibrillarin* (FBL) and total pri-miR487b determined by rt/qPCR using *RPLP0* or *U6* expression as reference as indicated. (B-F) Data are presented as mean ± SEM (n of at least 3). **P*<0.05, ***P*<0.01, ****P*<0.001 versus HUAF expression.

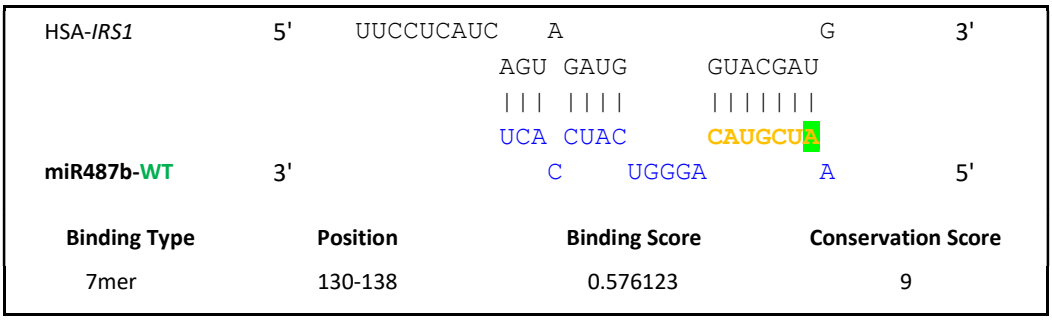


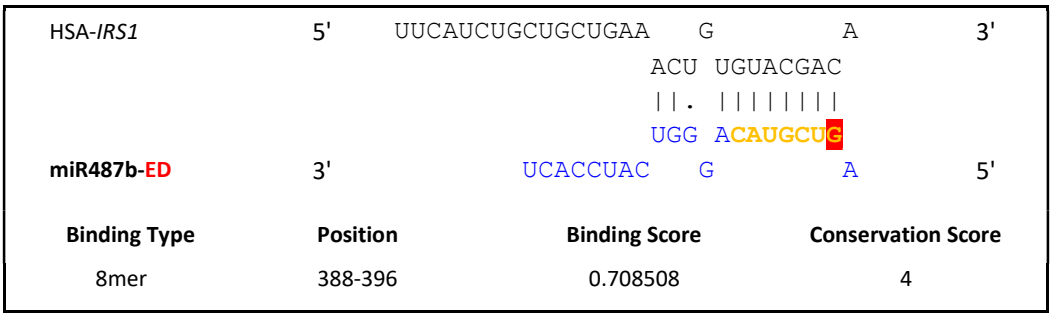


**Supplemental figure V: miR487b-WT and miR487b-ED binding sites in the 3'UTR of *IRS1*.** Predicted human *IRS1* and miR487b binding characteristics, including length of complementary nucleotides around the seed sequence (binding type), 3'UTR position to which the seed binds and binding and conservation score as predicted by Diana-MR-microT software (diana.imis.athena-innovation.gr). The seed sequences of the microRNAs are depicted in orange and the difference between WT and ED is highlighted.

| 6 individual miR487b-**ED** binding sites within HSA-*BMP1* | **Total binding score** 0.841079 |
|---|---|

HSA-*BMP1* **site 1** 5' GUACCGCAGCCGCC UG G 3'
UG CU GUACGACU
|| |. ||||||||
AC GG CAUGCUGA
**miR487b-ED** 3' UCACCU UG A 5'

| **Binding Type** | **Position** | **% strength of total** | **Conservation Score** |
|---|---|---|---|
| 8mer | 973-981 | ~23% | 3 |

HSA-*BMP1* **site 2** 5' UGAGCGCCACGACA C UG 3'
G UG CC UACGACU
| || || |||||||
C AC GG AUGCUGA
**miR487b-ED** 3' UCAC U UG AC 5'

| **Binding Type** | **Position** | **% strength of total** | **Conservation Score** |
|---|---|---|---|
| 7mer | 1312-1320 | ~14% | 9 |

HSA-*BMP1* **site 3** 5' AG CAUGAU UG AA 3'
AG GG GUG C GUACGACU
|| || .|| | ||||||||
UC CC UAC G CAUGCUGA
**miR487b-ED** 3' A UG GA 5'

| **Binding Type** | **Position** | **% strength of total** | **Conservation Score** |
|---|---|---|---|
| 8mer | 1312-1320 | ~35% | 8 |

HSA-*BMP1* **site 4** 5' CUUCGUCCUCC AACAA C 3'
AUGAC G ACGACU
||||| | ||||||
UACUG C UGCUGA
**miR487b-ED** 3' UCACC GGA A 5'

| **Binding Type** | **Position** | **% strength of total** | **Conservation Score** |
|---|---|---|---|
| 6mer | 2747-2755 | ~11% | 8 |

HSA-*BMP1* **site 5** 5' GAGUCCCAGCC A UG C 3'
UG GUG CC UACGAC
|| .|| || ||||||
AC UAC GG AUGCUG
**miR487b-ED** 3' UC C UG AC A 5'

| **Binding Type** | **Position** | **% strength of total** | **Conservation Score** |
|---|---|---|---|
| 6mer | 2933-2941 | ~7% | 6 |

HSA-*BMP1* **site 6** 5' UACA UCGACGGC A 3'
UGGA GCUCU UACGAC
|||| .|.|| ||||||
ACCU UGGGA AUGCUG
**miR487b-ED** 3' UC AC C A 5'

| **Binding Type** | **Position** | **% strength of total** | **Conservation Score** |
|---|---|---|---|
| 6mer | 3311-3319 | ~11% | 7 |

**Supplemental figure VI: Six distinct miR487b-ED binding sites found in *BMP1*.** Predicted human *BMP1* and miR487b-ED binding characteristics as in **Supplemental Figure V**. Six distinct miR487b-ED binding sites within the *BMP1* transcript result in a total Diana binding score of 0.841. Estimated contribution per binding site are presented as approximate percentage of total binding strength.

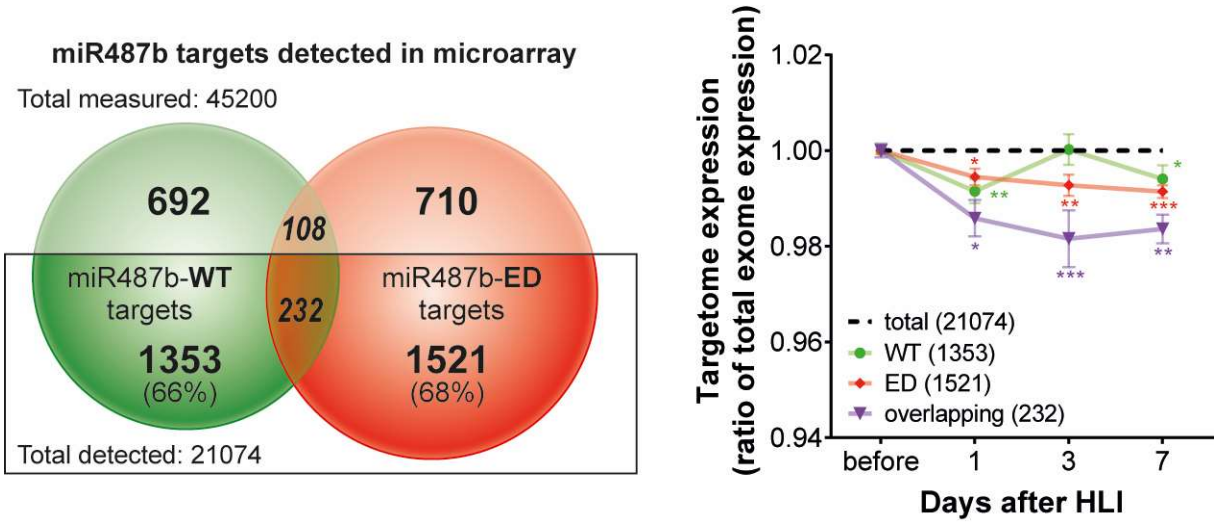


**Supplemental Figure VII. Expression of unedited and edited putative targetomes in the adductor muscle.** Schematic overview (left) of the number of putative target genes of miR487b-WT and miR487b-ED (green and red respectively) that were detected in whole-genome expression microArray performed on mRNA of total adductor muscle mRNA of the same mice used in previous HLI experiments. To the right, the fold change in average targetome expression of miR487b-WT and miR487b-ED (green and red respectively) and the overlapping targets (purple) after HLI are shown. Targetome expression was normalized to average expression of all genes detected and presented as mean ± SEM of at least 3 different mice per timepoint. *$P$<0.05, **$P$<0.01 ***$P$<0.001 compared to control whole-genome expression.

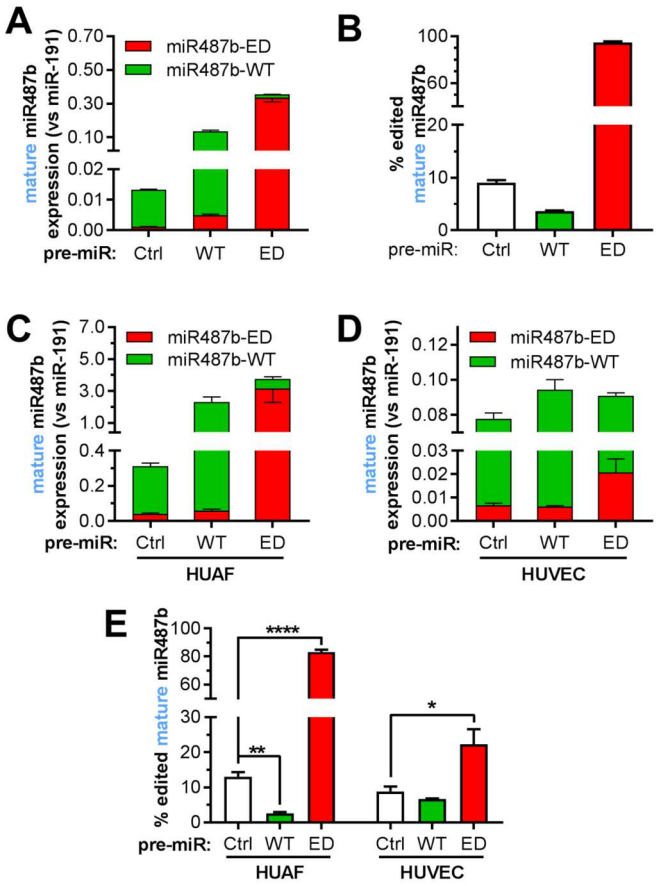


**Supplemental Figure VIII: MiR487b-WT and miR487b-ED overexpression in aortic rings and primary human fibroblasts and endothelial cells.** Additional aortic rings were incubated alongside the embedded rings with either pre-miR487b-WT, pre-miR487b-ED or control pre-miRNA for 7 days for quantification of overexpression. RNA was isolated from at least 20 rings originating from 6 different mouse aortas, which were pooled per treatment to provide sufficient yields. (**A**) Relative expression of mature miR487b-WT (green) and miR487b-ED (red) measured by rt/qPCR performed on aortic ring cDNA where miR191 was used as stable reference miRNA. (**B**) Percentage mature miR487b editing calculated from data presented in (**A**). (**A&B**) Data are presented as mean with SEM of technical triplicate. (**C&D**) Expression of mature miR487b-WT (green) and miR487b-ED (red) in cDNA isolated from HUAFs (**C**) and HUVECs (**D**) subjected to scratch-wound healing assay and treatment with 1nM of either pre-miR487b-WT, pre-miR487b-ED or negative control pre-miR. Quantification was done by rt/qPCR as before. Percentage mature miR487b editing calculated from data presented in (**C&D**). (**C-E**) Data are presented as mean ± SEM (n=3). **P*<0.05, ***P*<0.01, *****P*<0.0001 versus control pre-miRNA.

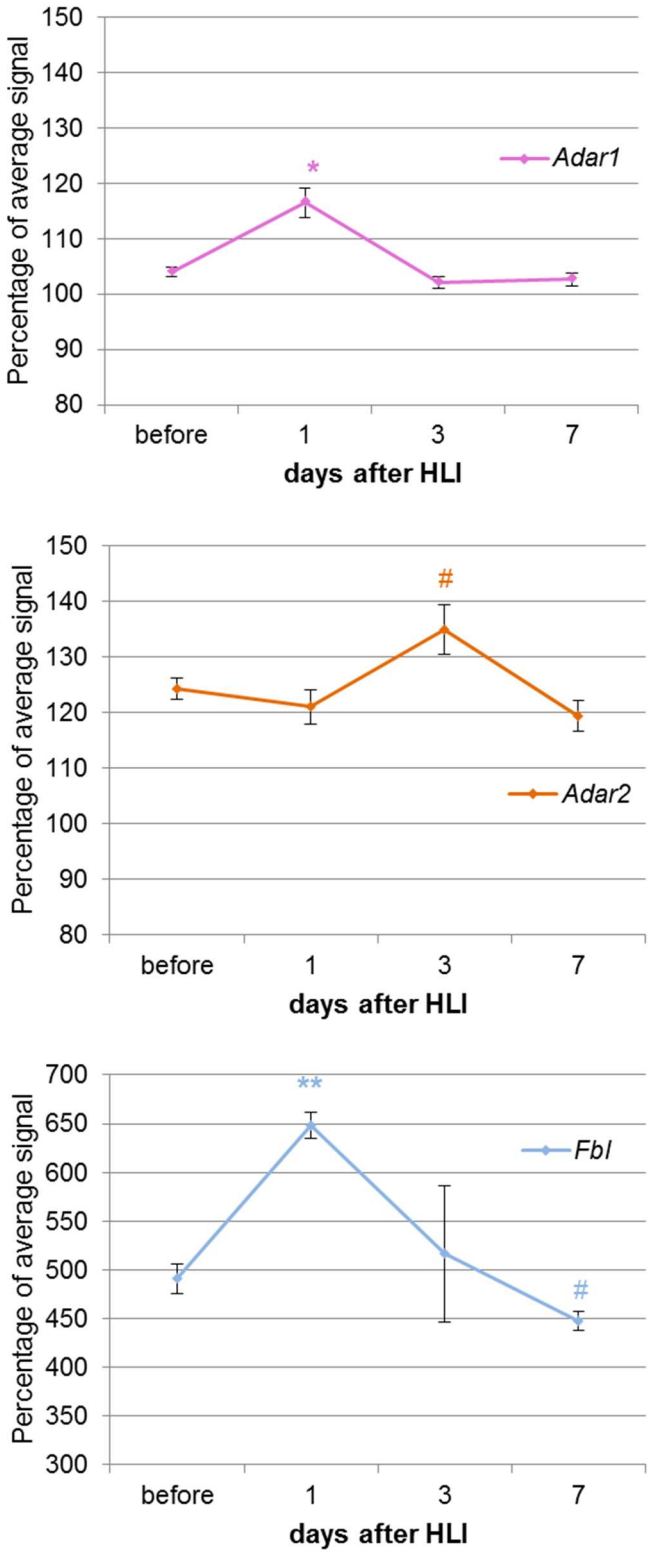


**Supplemental Figure IX: Murine *Adar1*, *Adar2* and *Fibrillarin* mRNA expression in whole genome analysis of the adductor muscle before and after induction of HLI.** Murine *Adar1*, *Adar2* and *Fibrillarin (Fbl)* mRNA expression extrapolated from a previously published whole genome expression microArray dataset (Nossent et al[7]). Expression was expressed as percentages of average signal and represented as mean ± SEM of at least 3 different mice per timepoint. #$P$<0.1, *$P$<0.05 vs before HLI.

## SUPPLEMENTAL REFERENCES


1. Criqui MH, Aboyans V. Epidemiology of peripheral artery disease. *Circ Res*. 2015;116:1509-1526
2. Welten SM, Bastiaansen AJ, de Jong RC, de Vries MR, Peters EA, Boonstra MC, Sheikh SP, La Monica N, Kandimalla ER, Quax PH, Nossent AY. Inhibition of 14q32 MicroRNAs miR-329, miR-487b, miR-494, and miR-495 increases neovascularization and blood flow recovery after ischemia. *Circ Res*. 2014;115:696-708
3. Dong ZW, Shao P, Diao LT, Zhou H, Yu CH, Qu LH. RTL-P: a sensitive approach for detecting sites of 2'-O-methylation in RNA molecules. *Nucleic Acids Res*. 2012;40:e157-e157
4. Aschenbrenner J, Marx A. Direct and site-specific quantification of RNA 2'-O-methylation by PCR with an engineered DNA polymerase. *Nucleic Acids Res*. 2016;44:3495-3502
5. Paraskevopoulou MD, Georgakilas G, Kostoulas N, Vlachos IS, Vergoulis T, Reczko M, Filippidis C, Dalamagas T, Hatzigeorgiou AG. DIANA-microT web server v5.0: service integration into miRNA functional analysis workflows. *Nucleic Acids Res*. 2013;41:W169-173
6. Mi H, Muruganujan A, Casagrande JT, Thomas PD. Large-scale gene function analysis with the PANTHER classification system. *Nat Protoc*. 2013;8:1551-1566
7. Nossent AY, Bastiaansen AJ, Peters EA, de Vries MR, Aref Z, Welten SM, de Jager SC, van der Pouw Kraan TC, Quax PH. CCR7-CCL19/CCL21 Axis is Essential for Effective Arteriogenesis in a Murine Model of Hindlimb Ischemia. *Journal of the American Heart Association*. 2017;6
8. Stellos K, Gatsiou A, Stamatelopoulos K, et al. Adenosine-to-inosine RNA editing controls cathepsin S expression in atherosclerosis by enabling HuR-mediated post-transcriptional regulation. *Nat Med*. 2016;22:1140-1150
9. Lamalice L, Le Boeuf F, Huot J. Endothelial cell migration during angiogenesis. *Circ Res*. 2007;100:782-794
10. Friedl P, Gilmour D. Collective cell migration in morphogenesis, regeneration and cancer. *Nat Rev Mol Cell Biol*. 2009;10:445-457
11. Baker M, Robinson SD, Lechertier T, Barber PR, Tavora B, D'Amico G, Jones DT, Vojnovic B, Hodivala-Dilke K. Use of the mouse aortic ring assay to study angiogenesis. *Nat Protoc*. 2011;7:89-104
12. Pfaffl MW. A new mathematical model for relative quantification in real-time RT-PCR. *Nucleic Acids Res*. 2001;29:e45